



Norwegian University of
Science and Technology

Effect of Low Temperature Tensile Properties on Crack Driving Force for Arctic Applications

Bjørn Augdal Dahl

Mechanical Engineering

Submission date: June 2016

Supervisor: Odd Magne Akselsen, IPM

Co-supervisor: Zhiliang Zhang, KT

Norwegian University of Science and Technology
Department of Engineering Design and Materials

Abstract

Many petroleum companies expand their activities further north towards the Arctic region, resulting in design temperatures down to $-60\text{ }^\circ\text{C}$, which is much lower than what is usual for most current petroleum installations. As properties of steels are temperature dependent, it is of great interest to evaluate the effects of low temperature on the crack driving force in steels. The present work investigates these effects numerically using finite element (FE) models of single-edge-notched-tension (SENT) specimens with crack depths $0.1 \leq a/W \leq 0.5$. The effects of Lüders strain, yield strength and crack depth on the crack tip opening displacement (CTOD) and the relation between CTOD and crack mouth opening displacement (CMOD) are studied, and it is shown that an increase in yield strength and Lüders strain, as a result of Arctic temperature, intensifies the crack driving force. It is also shown that the crack depth has very little influence on the effect of Lüders strain on the CTOD. An approximate model that can be used to estimate the CTOD based on yield strength, Lüders strain and loading is proposed for gross stress levels $\sigma_G/\sigma_y \leq 0.5$ and a crack depth $a/W = 0.5$. It is finally shown that the tensile properties have a more significant effect on the CTOD-CMOD relation than the crack depth for a SENT specimen.

Mange petroleumsselskaper utvider sine aktiviteter nordover mot arktiske områder. Dette fører til designtemperaturer ned til $-60\text{ }^\circ\text{C}$, noe som er mye lavere enn det som er vanlig for de fleste nåværende petroleumsinstallasjoner. Ettersom egenskapene til stål er temperaturavhengige, er det av stor interesse å evaluere effektene av lav temperatur på den drivende kraften for sprekkvekst i stål. Dette arbeidet undersøker disse effektene numerisk ved hjelp av elementmetoden med modeller av single-edge-notched-tension (SENT)-bruddprøver med sprekkdybder $0.1 \leq a/W \leq 0.5$. Effektene av Lüders tøyning, flytespenning og sprekkdybde på sprekkspissutvidelsen (CTOD) og sammenhengen mellom CTOD og sprekkmunningsutvidelsen (CMOD) er studert, og det er påvist at økt flytespenning og Lüders tøyning, som et resultat av arktisk temperatur, fører til økt drivende kraft for sprekkvekst. Det er også vist at sprekkdybden har liten innflytelse på effekten av Lüders tøyning på CTOD. Det er foreslått en omtrentelig modell som kan bli brukt til å estimere CTOD basert på flytespenning, Lüders tøyning og last for bruttospenningsnivåer $\sigma_G/\sigma_y \leq 0.5$ og sprekkdybde $a/W = 0.5$. Det er til slutt påvist at materialets strekkegenskaper har en større virkning på CTOD-CMOD-forholdet enn sprekkdybden for en SENT-prøve.

Preface

The work presented here is a Master's thesis written at Department of Engineering Design and Materials at Norwegian University of Science and Technology (NTNU). The thesis work is carried out as a part of SMACC (Studies of materials behavior for future cold climate applications), which is a research project with several industry partners, and with SINTEF and NTNU as research partners.

The author wishes to thank SINTEF for the opportunity to be introduced to the SMACC-project through an exciting and educational summer job. Thanks also to SINTEF and NTNU for the opportunity to be a part of the research project through the project and Master's thesis work.

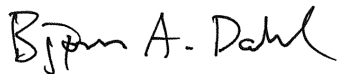
The author also wishes to thank the Research Council of Norway for funding of the research project through the Petromaks 2 Programme, Contract No.228513/E30. The financial support of SMACC from ENI, Statoil, Lundin, Total, JFE Steel Corporation, Posco, Kobe Steel, SSAB, Bredero Shaw, Borealis, Trelleborg, Nexans, Aker Solutions, FMC Kongsberg Subsea, Kværner Verdal, Marine Aluminium, Hydro and Sapa are also acknowledged.

A large part of this thesis is based on Dahl et al. (2016), which is written during the project and Master's thesis period. The paper was submitted to an international journal in May 2016. The author wishes to thank Odd Magne Akselsen, Zhiliang Zhang, Xiaobo Ren and Bård Nyhus for the great support and guidance during the work with the paper, project and Master's thesis.

The author also wishes to thank his family and friends for the support through all the years, both before and during the years of study.

Finally, a big thank goes to the author's girlfriend for the daily support at home. She has enriched the days by making the spare time be about other things than worrying about the studies.

Trondheim, June 9, 2016



Bjørn Augdal Dahl

Table of Contents

Abstract	i
Preface	iii
Table of Contents	v
List of Tables	vii
List of Figures	x
1 Introduction	1
2 Experimental work on low temperature tensile properties	5
3 Material model and numerical procedure	7
4 Results and discussion	11
4.1 Effect of yield stress	11
4.2 Effect of Lüders strain	13
4.3 Approximate CTOD model	13
4.4 Influence of crack depth on Lüders strain effect	22
4.5 Effects on the CMOD-CTOD relationship	27
5 Conclusion	31
Bibliography	33
Appendix	37
Master thesis contract	37
Risk assessment	41
Effect of low temperature tensile properties on crack driving force for Arctic applications	47

List of Tables

3.1 Constant material parameters.	9
---	---

List of Figures

2.1	Engineering stress-strain curves of a 420 MPa steel at different temperatures. Taken from Ren et al. (2015).	6
3.1	Illustration of a SENT specimen with dimensions.	7
3.2	Global mesh for a/W from 0.1 to 0.5 in (a) to (e) respectively.	9
3.3	Local finite element mesh showing the crack tip region. The node where CTOD is measured is marked by the circle.	10
3.4	Illustration of a material model showing the three different parts of the stress-strain curve.	10
4.1	Examples of some of the model materials studied.	12
4.2	CTOD versus gross stress level with 300 MPa to 800 MPa yield strengths and Lüders strains ranging from 0 to infinite in (a) to (f) respectively.	14
4.3	CTOD versus gross stress level with 0, 1 %, 2 %, 3 %, 5 % and infinite Lüders strains and yield strengths ranging from 300 MPa to 800 MPa in (a) to (f) respectively.	15
4.4	Proposed relations according to Eq. 4.2 as a function of yield strength normalized by a reference stress of 420 MPa together with the values for the b -parameter obtained by fitting the proposed relation in Eq. 4.1 to the numerical results shown in Figures 4.2 and 4.3.	17
4.5	Comparison between Eq. 4.4 and the values for A from the fitting of Eq. 4.3 to the numerical results.	18
4.6	Proposed relations according to Eqs. 4.3 and 4.4 as a function of yield strength normalized by a reference stress of 420 MPa together with the values for the d -parameter obtained by fitting the proposed relation in Eq. 4.1 to the numerical results shown in Figures 4.2 and 4.3.	19

4.7	Proposed temperature dependent relation according to Eqs. 4.1, 4.2, 4.3 and 4.4 between CTOD and applied gross stress level in the SENT specimen compared to numerical results at (a) 0 °C, (b) –30 °C, (c) –60 °C and (d) –90 °C.	20
4.8	Comparison between CTOD curves estimated using the proposed CTOD model at four different temperatures.	21
4.9	CTOD versus gross stress level divided by $1 - a/W$ with 0, 0.5 %, 1 %, 2 %, 3 %, 5 % and infinite Lüders strains and a/W ranging from 0.1 to 0.5 in (a) to (e) respectively. The yield strength is 400 MPa.	23
4.10	CTOD versus gross stress level divided by $1 - a/W$ with 0, 0.5 %, 1 %, 2 %, 3 %, 5 % and infinite Lüders strains and a/W ranging from 0.1 to 0.5 in (a) to (e) respectively. The yield strength is 700 MPa.	24
4.11	CTOD versus global strain with a/W ranging from 0.1 to 0.5 and 1 % to 5 % Lüders strain in (a) to (d) respectively. The yield strength is 400 MPa.	25
4.12	CTOD versus global strain with a/W ranging from 0.1 to 0.5 and 1 % to 5 % Lüders strain in (a) to (d) respectively. The yield strength is 700 MPa.	26
4.13	δ_L versus a/W using materials with four different Lüders strains and two yield strengths.	27
4.14	CTOD-CMOD results from FE analyses with 400 MPa and 700 MPa yield strength materials with Lüders strains equal to 0 and 2 % and a/W ranging from 0.1 to 0.5 in (a) to (e) respectively. The top and rightmost axes are the CMOD and CTOD respectively normalized by the crack depth a to facilitate comparison between figures (a) to (f).	29

Chapter 1

Introduction

The exploitation of hydrocarbons is continuously moving into new areas and harsher environments. Many petroleum companies are expanding their activities further north, where a considerable part of the undiscovered oil and gas resources is expected to exist (Gautier et al., 2009). Consequently the structures built must be able to withstand the low temperatures present in the Arctic climate. Most structural materials have different behavior in such low temperatures, and this must be accounted for when designing and constructing structures to avoid accidents related to structural failure.

Much research has been carried out to study the behavior of steels in changing temperatures. The most obvious temperature dependent parameter is the yield strength, which for most steels increase with decreasing temperature (Akselsen et al., 2012, 2011; Baek et al., 2002; Costin and Duffy, 1979; Eldin and Collins, 1951; Heier et al., 2013; Marais et al., 2012; Ren et al., 2015; Ritchie et al., 1973; Robertson et al., 2007; Sieurin and Sandström, 2006; Sorem et al., 1991; Wilson et al., 1980). Another temperature dependent property is the ductile-to-brittle transition (DBT) in steels. Due to the DBT, many steels become brittle when the temperature is sufficiently decreased, but the DBT is however not in the scope of this study.

Many steels, and also other materials, experience so-called Lüders and Lüders-like instabilities. These instabilities are associated with unpinning of dislocations from nitrogen and carbon atmospheres and dislocation multiplication, and they result in macroscopic inhomogeneous deformation (Cottrell and Bilby, 1949; Hahn, 1962; Hallai and Kyriakides, 2013; Johnson, 2013; Liu et al., 2015; Marais et al., 2012; Mazière and Forest, 2013). The Lüders instability is in uniaxial tensile tests observed as nearly horizontal stress plateaus, called Lüders plateaus, in the stress-strain curves after reaching the elastic limit of the material. This instability can be physically observed as localized deformation bands, called Lüders bands, propagating on the surface of uniaxial tensile tests. Structural steels often show this behavior. The amount of plastic straining occurring due to the Lüders instability

is often called Lüders strain. Studies have shown that the Lüders strain is both rate and temperature dependent, and decreasing temperature is often associated with larger Lüders strain (Heier et al., 2013; Johnson, 2013; Marais et al., 2012; Ren et al., 2015; Tsuchida et al., 2006).

The fracture toughness of a material is often measured by using fracture mechanics tests, and is described by a single parameter, such as a critical stress intensity factor (K), crack tip opening displacement (CTOD, δ) or J -integral, depending on if it is a linear elastic or elastoplastic dominated fracture. The fracture toughness of steels is usually reduced when decreasing the temperature (Costin and Duffy, 1979; Ritchie et al., 1973; Sieurin and Sandström, 2006; Sorem et al., 1991; Wilson et al., 1980; Zerbst et al., 2014).

The fracture toughness can be interpreted as a measure of the ability of a material to resist fracture, while the crack driving force, on the other hand, can be defined as the force which opens the crack. The fracture toughness can be regarded as the critical level of crack driving force, and the same way as a critical CTOD can be a measure of the fracture toughness, the CTOD is often used as a measure of the crack driving force which changes with loading. Due to temperature dependent material parameters, decreasing temperature is assumed to have an effect on the crack driving force (Østby et al., 2013). The goal of this work is hence to study the effect of low temperature material properties of steels, as expected in Arctic applications, on the crack driving force by performing finite element analyses. This effect is studied by simulating fracture tests of a single-edge-notched-tension (SENT) specimen with a material model where the temperature dependent material parameters can be changed. The CTOD is used as a measure of the crack driving force. A SENT specimen is studied because it is used as a fracture specimen to estimate fracture toughness of steels used for pipeline applications where other specimen types give unnecessarily conservative results, such as for girth welds in pipes (Det Norske Veritas, 2006; Nyhus et al., 2003).

The results will be utilized to propose approximate CTOD models that can be used to estimate the crack driving force in a SENT specimen at low temperatures by using only tensile properties of the material. This can for instance also be useful for estimating the CTOD or maximum stress allowed in a cracked pipeline in Arctic climate.

The approximate CTOD models will be based on a SENT specimen with a constant crack depth a/W , but the effect of crack depth will be investigated to confirm that the results are transferable to SENT specimens with other crack depths. It is known that increasing crack depth yields a larger crack driving force (Østby et al., 2013). However, the influence of crack depth on the effect of Lüders strain on the crack driving force is not found in literature. This is thus further investigated, as the proposed CTOD model can be modified to be used for varying crack depths as long as the effect of Lüders strain on CTOD is not changing behavior with the crack depth.

Finally, the relationship between CTOD and crack mouth opening displacement (CMOD) is studied. CMOD is very easy to measure and is thus often used directly to calculate the CTOD in experimental fracture testing with single-edge-

notched-bending (SENB) specimens. With SENT specimens this may not be as straightforward, but if the tensile properties of the material have no or little effect on the CTOD-CMOD relationship, it should be possible to make equations that estimate the CTOD based on measuring just the CMOD, even if the yield strength and Lüders strain change, for instance due to variations in temperature.

Experimental work on low temperature tensile properties

The recent work by Ren et al. (2015) and Østby et al. (2013) has presented tensile properties of a 420 MPa steel at different temperatures ranging from 0 °C down to -90 °C. They tested both base material, weld metal and weld thermal simulated microstructure of steel. Smooth round specimens with gauge diameters between 10 mm and 12 mm were used for testing the base material, and they were loaded with a strain rate of $8 \times 10^{-4} \text{ s}^{-1}$. An example of engineering stress-strain results is shown in Figure 2.1.

The results in Figure 2.1 show that both the yield strength and the Lüders strain increase with decreasing temperature. The yield strength and Lüders strain from 0 °C to -90 °C are ranging from approximate 470 MPa and 1.4 % to 540 MPa and 2.2 % respectively.

Tensile properties at low temperatures cannot always be obtained due to cost or practical reasons, and several corrections for calculating tensile properties at temperatures lower than room temperature are thus proposed in literature (British Standards Institution, 2013; Ren et al., 2015; Østby et al., 2013).

Ren et al. (2015) introduced a modified version of the correction proposed by British Standards Institution (2013) based on their results from tensile tests on a 420 MPa steel:

$$\sigma_{y,T} = 420 \text{ MPa} + 0.73 \text{ MPa} \left(\frac{10^5}{491 + 1.8T} - 137 \right) \quad (2.1)$$

where $\sigma_{y,T}$ is the yield strength in MPa at temperature T in °C. They proposed in addition a relation between Lüders strain and temperature:

$$\varepsilon_L = 0.0142 \exp(-0.005T) \quad (2.2)$$

where T is the temperature in °C and ε_L is the Lüders strain. Eqs. 2.1 and 2.2 are expected to be valid for the tested temperature range from -90 °C to 0 °C.

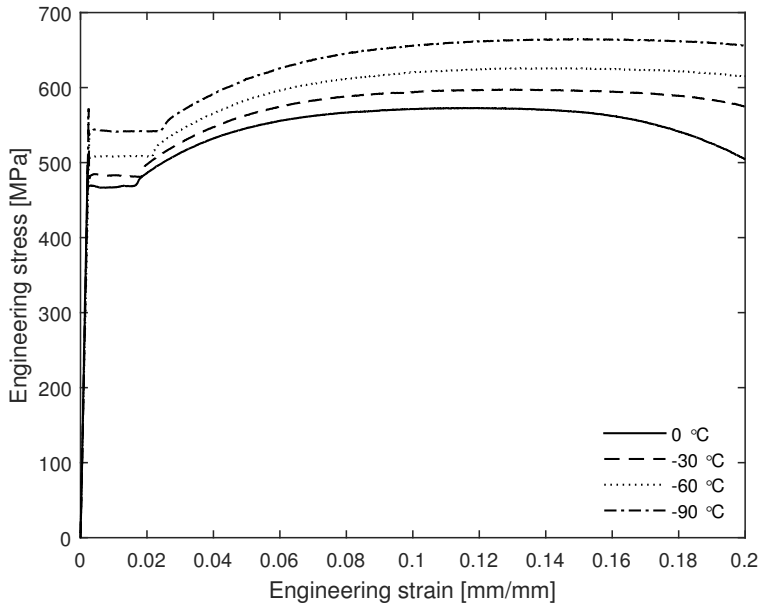


Figure 2.1: Engineering stress-strain curves of a 420 MPa steel at different temperatures. Taken from Ren et al. (2015).

The effect of the low temperature tensile properties on the crack driving force will be numerically studied in the following, where Eqs. 2.1 and 2.2 will be used to estimate the yield strength and Lüders strain present at different temperatures.

Material model and numerical procedure

The numerical simulations were performed using the commercial finite element program Abaqus 6.14 (Dassault Systèmes Simulia Corp., 2014). The finite element (FE) models studied are two-dimensional plane strain SENT specimens. The symmetry is utilized by modelling only half of the specimen. The width of the specimen is 50 mm, and the length is determined using a recommended practice (Det Norske Veritas, 2006): $L/W = 10$, where W is the specimen width and L is the specimen length. The first analyses use a constant crack depth: $a/W = 0.5$, where a is the crack depth as illustrated in Figure 3.1. The subsequent analyses use models with varying a/W from 0.1 to 0.5.

Large plastic deformations are expected at the crack tip, and the crack is modelled as an initially blunted crack with a tip radius of $10\ \mu\text{m}$. The large-displacement formulation that accounts for nonlinear geometric effects (NLGEOM) is used in the analyses. The finite element meshes consist of 8-node plane strain CPE8 elements. The meshes are refined around the crack tip where large strain gradients are ex-

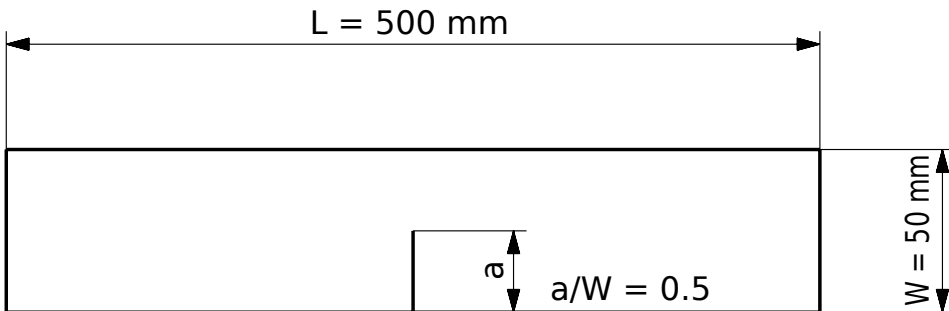


Figure 3.1: Illustration of a SENT specimen with dimensions.

pected, which is the primary area of interest in this study. There are 10 elements along the edge of the crack tip. The meshes and crack tip radius were determined based on a convergence study with varying mesh densities, element types and crack tip radii. The final finite element meshes for different a/W are shown in Figure 3.2. Figure 3.3 shows the local mesh in the crack tip region.

A uniform displacement is applied on the end of the half specimen to simulate the tension of a clamped SENT specimen. The displacement is set as high as needed to make the ligament net section stress exceed the yield stress of the material.

An elastoplastic material model based on uniaxial tensile tests of the steel in Ren et al. (2015) is used in the analyses. The material displays isotropic linear elasticity and J_2 -plasticity with isotropic hardening, while an amount of Lüders straining is added in the transition between the elastic and plastic behavior. The Lüders behavior is modelled as a simplified horizontal Lüders plateau in the plastic stress-strain curve. There are many proposals for more realistic modelling of the Lüders instability in literature, which for instance include strain drops or strain softening (Hallai and Kyriakides, 2013; Liu et al., 2015; Marais et al., 2012; Mazière and Forest, 2013; Shioya and Shioiri, 1976; Tsukahara and Iung, 1998; Wenman and Chard-Tuckey, 2010; Zhang et al., 2007), but the simplified flat Lüders plateau is assumed to give a sufficient approximation to the material behavior in the present analysis. This is verified by doing analyses using a material model similar to the model in Mazière and Forest (2013). The modelled stress-strain curve is fitted to true stress-strain data from the uniaxial tensile tests in Ren et al. (2015), and it is then modified to create several similar materials with varying parameters such as yield stress and Lüders strain. The material can be described by

$$\sigma = \begin{cases} E\varepsilon & \text{if } 0 \leq \varepsilon < \frac{\sigma_y}{E} \\ \sigma_y & \text{if } \frac{\sigma_y}{E} \leq \varepsilon < \frac{\sigma_y}{E} + \varepsilon_L \\ \sigma_y + K \left(\varepsilon - \left(\frac{\sigma_y}{E} + \varepsilon_L \right) \right)^n & \text{if } \varepsilon \geq \frac{\sigma_y}{E} + \varepsilon_L \end{cases} \quad (3.1)$$

in uniaxial tension, where σ is the uniaxial stress, E is the Young's modulus, ε is the uniaxial strain, σ_y is the yield stress, ε_L is the Lüders strain, K is a strength coefficient and n is the strain hardening exponent. For loads and deformations in the two-dimensional plane, the Poisson's ratio ν is also needed. The yield stress and Lüders strain are the temperature dependent parameters to be studied. The constant material parameters are summarized in Table 3.1, where K and n are determined by fitting Eq. 3.1 to the true stress-strain data from the uniaxial tensile testing in Ren et al. (2015). Eq. 3.1 divides the stress-strain curve into three parts: the linear elastic part, Lüders plateau and plastic hardening, as illustrated in Figure 3.4. As only quasi-static simulations are performed, there are no rate dependencies in the material model.

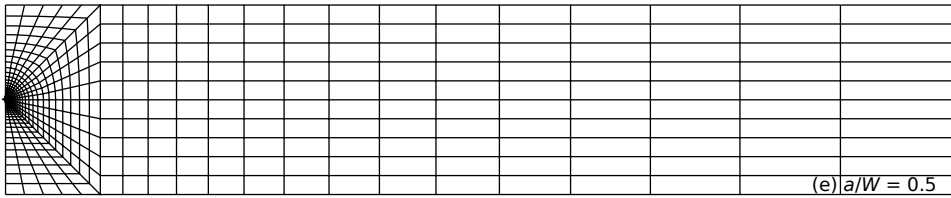
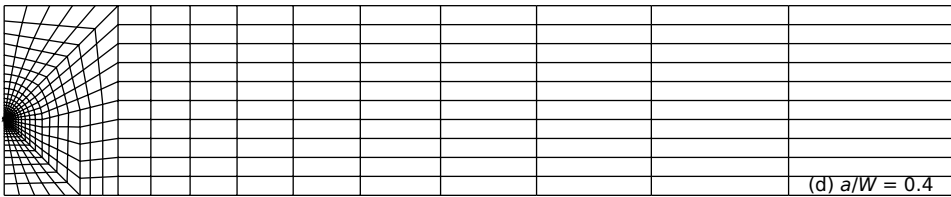
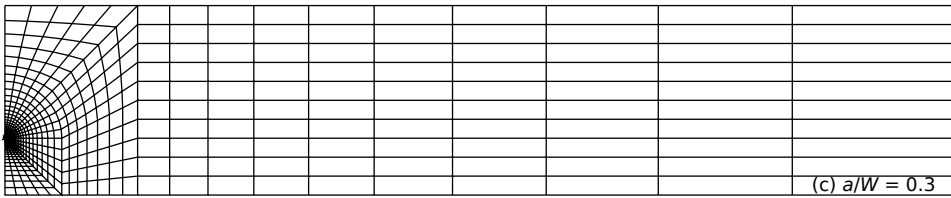
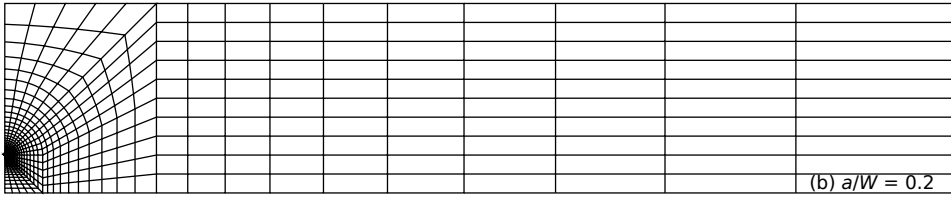
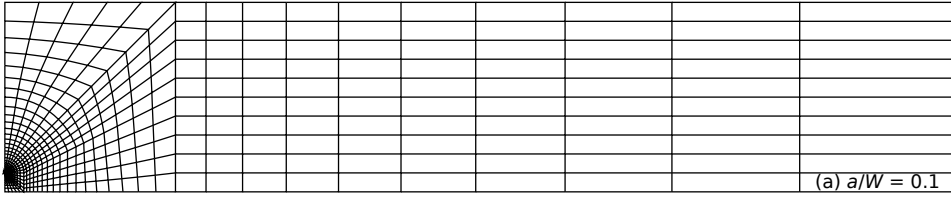


Figure 3.2: Global mesh for a/W from 0.1 to 0.5 in (a) to (e) respectively.

Table 3.1: Constant material parameters.

E	ν	K	n
210 GPa	0.3	685 MPa	0.576

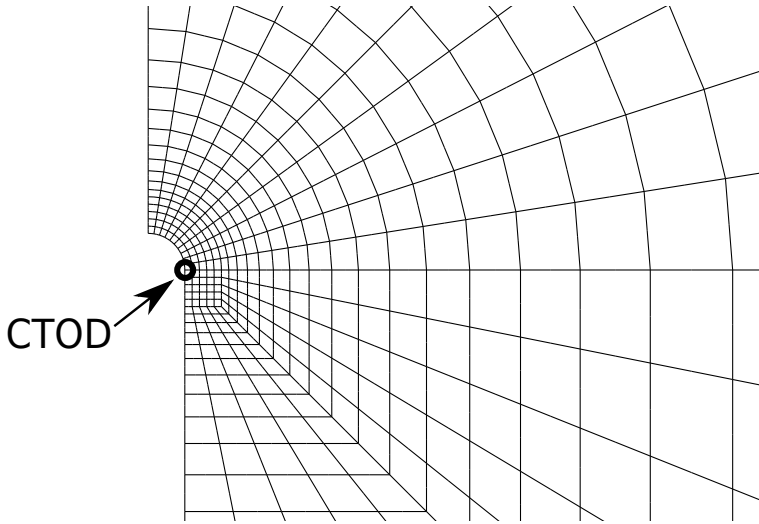


Figure 3.3: Local finite element mesh showing the crack tip region. The node where CTOD is measured is marked by the circle.

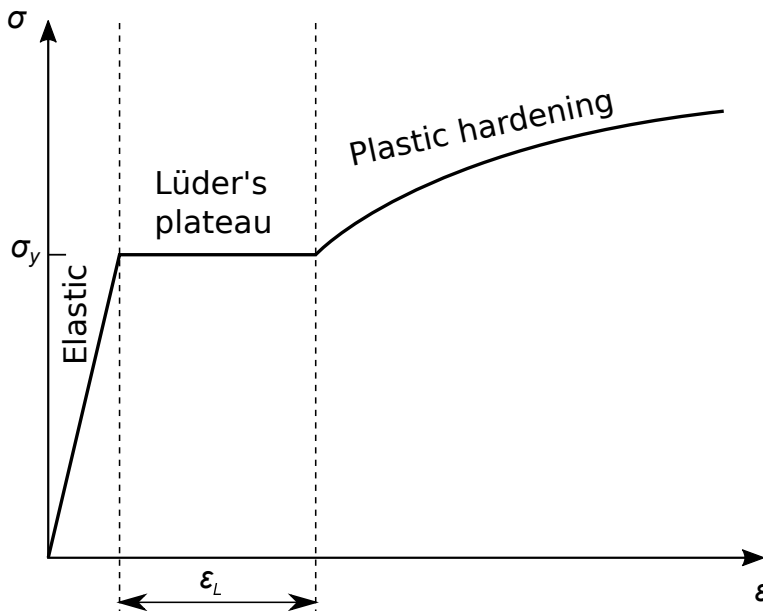


Figure 3.4: Illustration of a material model showing the three different parts of the stress-strain curve.

Results and discussion

To study how temperature dependent material properties affect the crack driving force, different analyses were performed where the parameters of interest were studied individually, and thereafter their combined effect was investigated. This study focuses on the effects of varying yield strength and Lüders strain on the CTOD. The CTOD is measured as twice the opening displacement of the fixed node in the transition point between the semicircular crack tip edge and the straight crack surface, as shown by the circle in Figure 3.3, which is equivalent to the initially 90 degree intercept method. The same procedure using a fixed node to calculate CTOD has been utilized in Eikrem et al. (2007); Liu et al. (2008); Thaulow et al. (2004); Xu et al. (2009, 2010). The results will be used to propose approximate CTOD models that can be utilized to estimate the CTOD based on given loadings and temperatures.

The influence of crack depth will be investigated using the same procedure, but with FE models with a/W varying from 0.1 to 0.5. The influence of a/W on the effect of Lüders strain on CTOD will be studied. Finally, the effect of crack depth, yield strength and Lüders strain on the CTOD-CMOD relation for SENT specimens will be investigated. The CMOD is measured as twice the opening displacement of the node at the leftmost bottom corner of the FE model.

4.1 Effect of yield stress

The effect of yield stress was studied by keeping the other parameters constant. Analyses with different yield stresses were performed with different levels of Lüders strain. A total of 36 analyses were performed to produce the following results, where 6 different yield stress levels, 300, 400, 500, 600, 700 and 800 MPa, were tested with 6 different levels of Lüders strain ranging from 0 to infinite. Examples of plastic uniaxial material responses are shown in Figure 4.1, where four materials with 400, 500, 600 and 700 MPa yield strength and 0, 1 %, 3 % and infinite Lüders strain respectively are displayed.

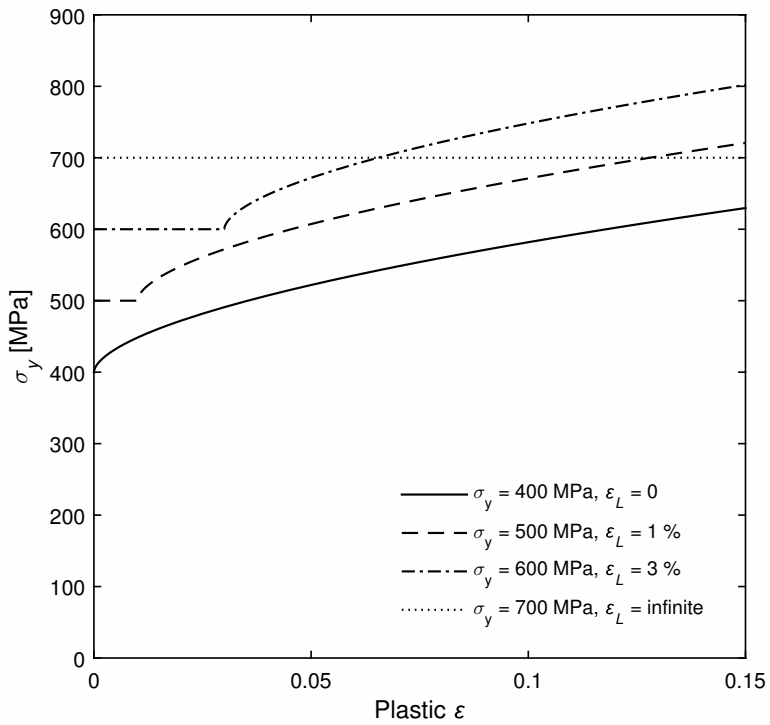


Figure 4.1: Examples of some of the model materials studied.

The CTOD results are plotted versus the gross stress level in each case in Figure 4.2. The gross stress level is defined as σ_G/σ_y , where σ_G is the gross stress defined as $\sigma_G = F_{\parallel}/(Wt)$, where F_{\parallel} is the longitudinal reaction forces at the specimen end, W is the specimen width and t is the specimen thickness. These results show that increasing yield stress results in increased CTOD at the same σ_G/σ_y . This can be expected as the same relative stress level corresponds to higher stresses and thus higher elastic strains in materials with higher yield strengths. This leads to a larger elastic deformation and hence a larger CTOD at the same relative stress level for a material with higher yield stress.

4.2 Effect of Lüders strain

The effect of the temperature dependent Lüders strain was studied by changing the amount of Lüders strain in the material model, while keeping the other parameters constant. This is the same as changing the length of the Lüders plateau in the uniaxial stress-strain curve. A total of 36 analyses were performed to produce the following results, where 6 different Lüders strains, 0, 1, 2, 3, 5 % and infinite, were tested with 6 different levels of yield stress ranging from 300 to 800 MPa.

The results from the simulations are shown in Figure 4.3, where the CTOD is plotted against the gross stress level. These are the same results as in Figure 4.2, but rearranged so that the effect of Lüders strain can be more easily studied. The results indicate that increasing Lüders strain, for instance caused by decreasing temperature, yields a larger CTOD, and hence a larger crack driving force, for a given loading. This can be explained due to the larger plastic deformation allowed by a material with larger Lüders strain. Figure 4.3 also indicates that the effect of Lüders strain on the CTOD is more evident at larger stress levels due to the difference in allowed plastic deformation. It should also be noted that the effect approaches a maximum for very large Lüders strains, as the curves approach the one for the material with infinite Lüders strain. The material with infinite Lüders strain corresponds to a material which displays perfect plasticity.

4.3 Approximate CTOD model

The results from the previous sections clearly show that the tensile properties have an effect on the crack driving force. These results will be utilized to create an approximate model that can be used for estimating the crack driving force in terms of CTOD based on yield strength and Lüders strain. This model will later in this section be coupled to the effect of temperature on the yield strength and Lüders strain according to Eqs. 2.1 and 2.2. The model can thus be used to estimate the CTOD in a SENT specimen based on loading and temperature when the effect of temperature on the tensile properties are known.

Based on the results in the previous sections the following relation between

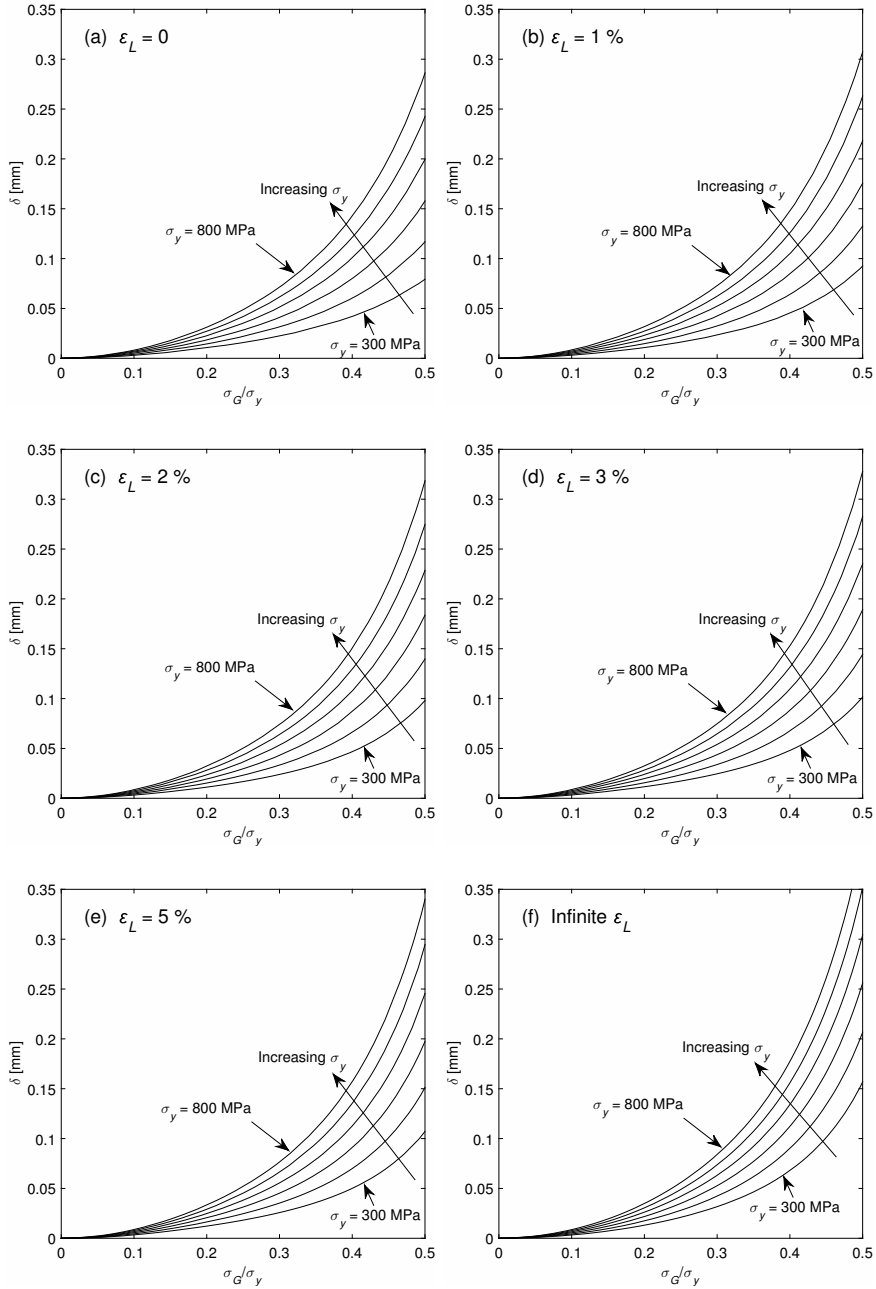


Figure 4.2: CTOD versus gross stress level with 300 MPa to 800 MPa yield strengths and Lüders strains ranging from 0 to infinite in (a) to (f) respectively.

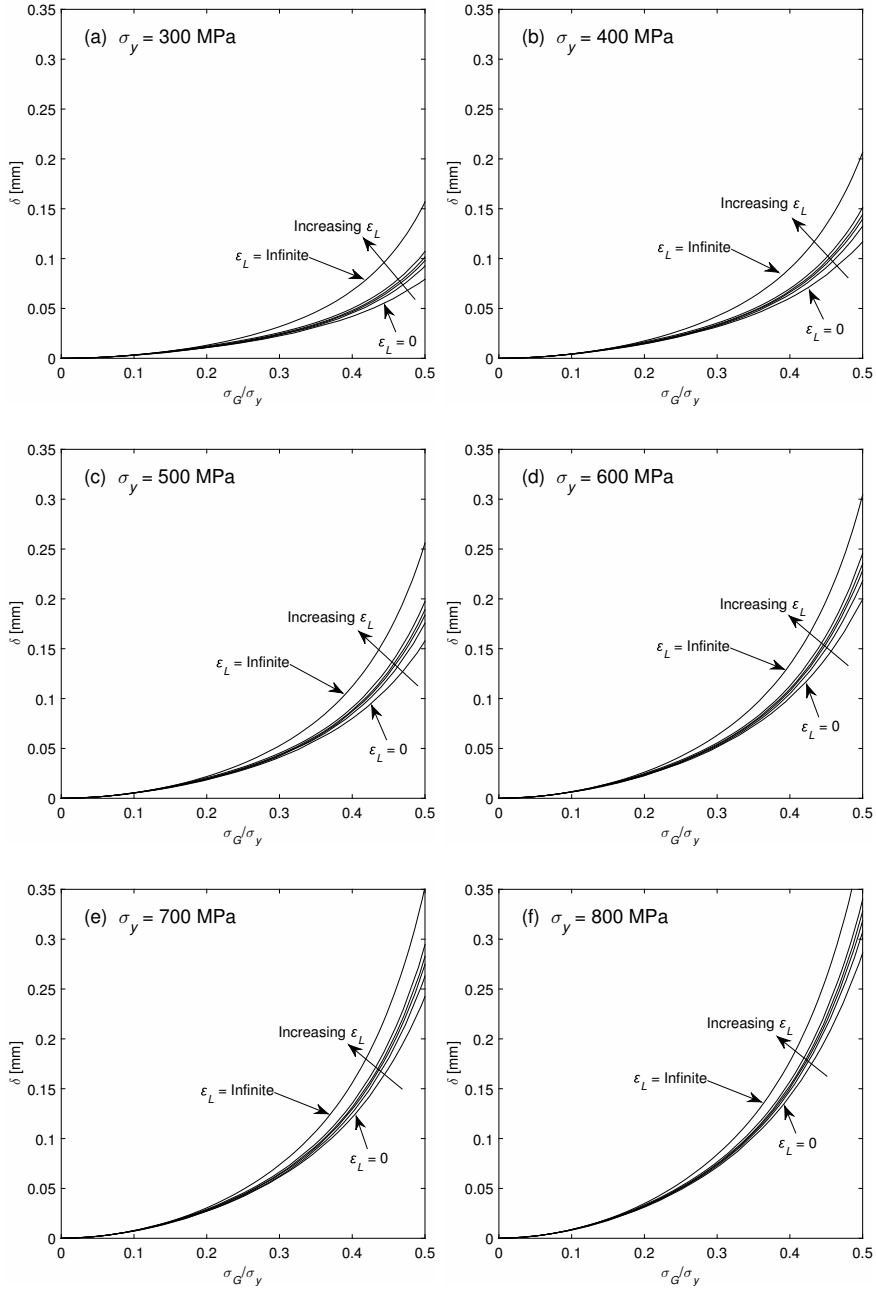


Figure 4.3: CTOD versus gross stress level with 0, 1%, 2%, 3%, 5% and infinite Luders strains and yield strengths ranging from 300 MPa to 800 MPa in (a) to (f) respectively.

CTOD and gross stress level is proposed:

$$\frac{\delta}{\delta_0} = b \left[\exp \left(d \frac{\sigma_G}{\sigma_y} \right) - 1 \right] \quad (4.1)$$

where δ_0 is a reference CTOD equal to 0.25 mm, which is a minimum required CTOD when applicable according to Standard Norge (2008). b and d are functions of yield stress and Lüders strain. Values for b and d in Eq. 4.1 were found by fitting the proposed relation to the numerical results shown in Figures 4.2 and 4.3, and based on these results the following relation for b is proposed:

$$b = \begin{cases} \left(23.4 \frac{\sigma_y}{\sigma_0} + 2.7 \right) \times 10^{-3} & \text{if } \varepsilon_L = 0 \\ \left(23.2 \frac{\sigma_y}{\sigma_0} - 1.1 \right) \times 10^{-3} & \text{if } 0 < \varepsilon_L \leq 1\% \\ \left(21.6 \frac{\sigma_y}{\sigma_0} - 0.6 \right) \times 10^{-3} & \text{if } 1\% < \varepsilon_L \leq 5\% \end{cases} \quad (4.2)$$

where b is a function of the yield stress normalized by a reference stress (σ_0) equal to 420 MPa, which is the specified minimum yield strength (SMYS) for many construction steels. As Figure 4.3 suggests, the effect of Lüders strain is evident, and it is thus accounted for in Eq. 4.2 by dividing the equation into three separate parts, where the first part is valid for materials showing no Lüders behavior, the second part is valid for Lüders strains below 1%, and the third part is valid for larger Lüders strains up to 5%. This partitioning of Eq. 4.2 helps estimating the CTOD more precisely for various levels of Lüders strain. The proposed relation for b as a function of σ_y/σ_0 is shown in Figure 4.4 together with the values for b according to the fitting of Eq. 4.1 to the numerical results.

Based on the values for d found by fitting Eq. 4.1 to the numerical results, the following relation is proposed:

$$d = \begin{cases} -0.51 \left(\frac{\sigma_y}{\sigma_0} \right)^2 + 1.97 \frac{\sigma_y}{\sigma_0} + 4.52 & \text{if } 0 \leq \varepsilon_L < 1\% \\ -0.33 \left(\frac{\sigma_y}{\sigma_0} \right)^2 + 1.17 \frac{\sigma_y}{\sigma_0} + A & \text{if } 1\% \leq \varepsilon_L \leq 5\% \end{cases} \quad (4.3)$$

where d is a function of yield strength normalized by the reference stress of 420 MPa. d is dependent on the amount of Lüders strain, and A is a function of Lüders strain. Similar to Eq. 4.2, the partitioning of Eq. 4.3 into two Lüders strain ranges helps estimating the CTOD more precisely for various levels of Lüders strain. Based on the fitting of Eq. 4.3 to the values for d found by fitting Eq. 4.1 to the numerical results, the following relation between A and ε_L is proposed:

$$A = \frac{6.025}{1 + 0.106 \exp(-58\varepsilon_L)} \quad (4.4)$$

The proposed relation between A and ε_L is shown in Figure 4.5 together with the values for A , which were found by fitting the relation from Eq. 4.4 to the

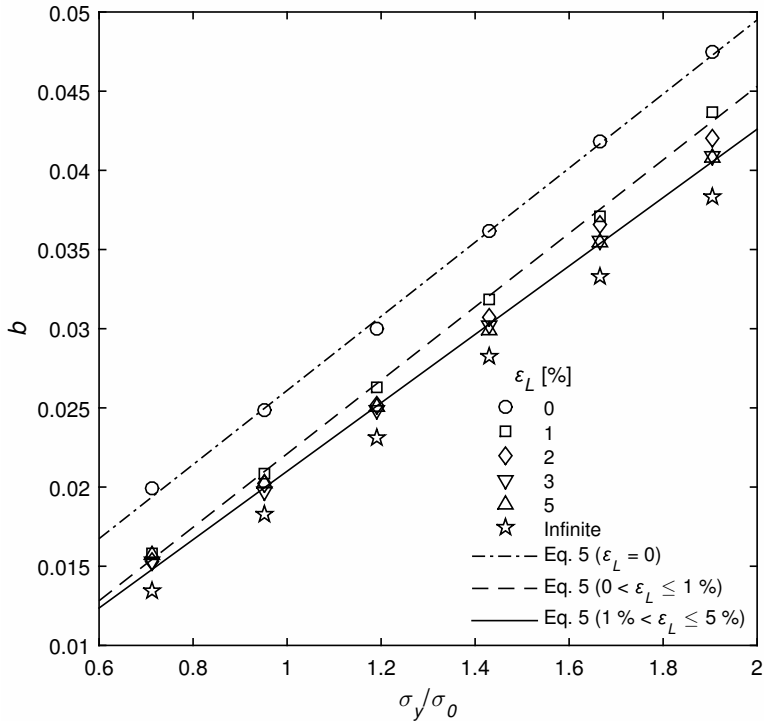


Figure 4.4: Proposed relations according to Eq. 4.2 as a function of yield strength normalized by a reference stress of 420 MPa together with the values for the b -parameter obtained by fitting the proposed relation in Eq. 4.1 to the numerical results shown in Figures 4.2 and 4.3.

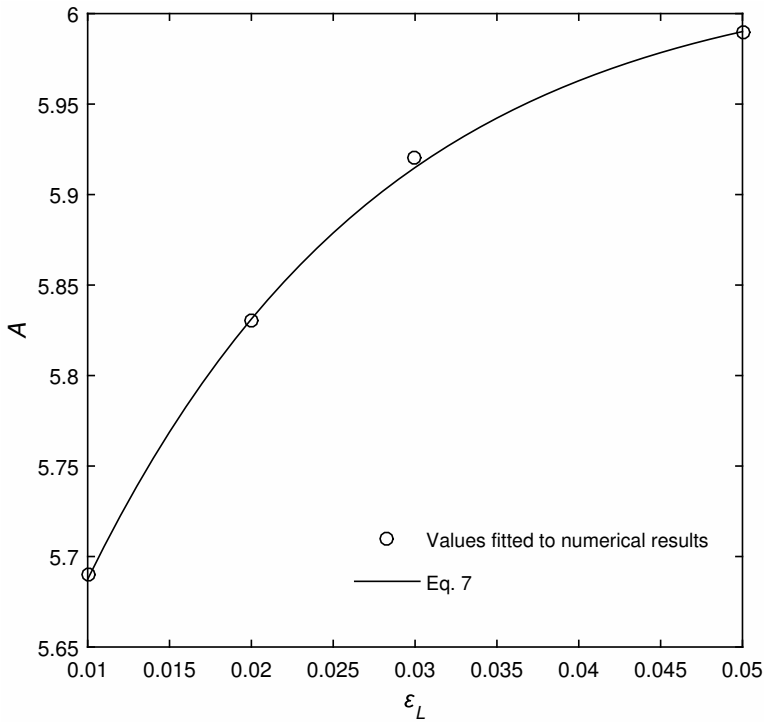


Figure 4.5: Comparison between Eq. 4.4 and the values for A from the fitting of Eq. 4.3 to the numerical results.

numerical results. The proposed relation for d in Eq. 4.3 using the calculated values for A according to Eq. 4.4 is shown in Figure 4.6 as a function of yield stress normalized by the reference stress together with the values for d according to the fitting of Eq. 4.1 to the numerical results.

The model described by the proposed relations in Eqs. 4.1, 4.2, 4.3 and 4.4 are compared to numerical results by coupling the model to the effect of temperature on the tensile properties. This is done by varying the yield strength and Lüders strain in the model material according to Eqs. 2.1 and 2.2 respectively at four different temperatures. The temperatures used are the same as during the experimental tensile tests in Ren et al. (2015). The comparison between the estimated and the numerical results is shown in Figure 4.7, where the normalized CTOD is plotted versus the applied gross stress level. The estimated results for the four different temperatures are compared in Figure 4.8. The gross stress levels are calculated as the gross stress divided by the estimated yield stresses according to Eq. 2.1 at the respective temperatures.

Figures 4.7 and 4.8 indicate that the proposed relations can be used to estimate the CTOD at different temperatures quite accurately for the material model used in this study. The proposed CTOD model utilizes known temperature dependent

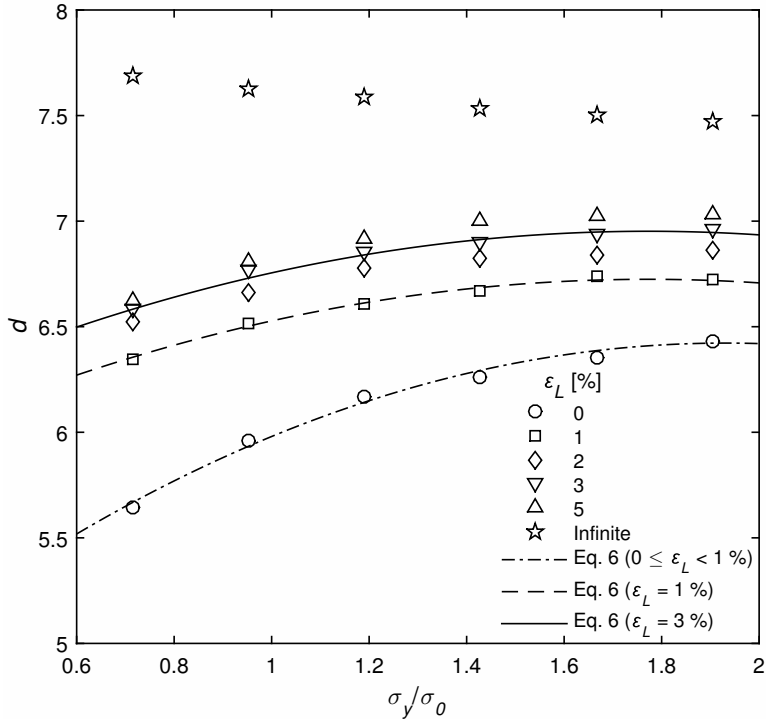


Figure 4.6: Proposed relations according to Eqs. 4.3 and 4.4 as a function of yield strength normalized by a reference stress of 420 MPa together with the values for the d -parameter obtained by fitting the proposed relation in Eq. 4.1 to the numerical results shown in Figures 4.2 and 4.3.

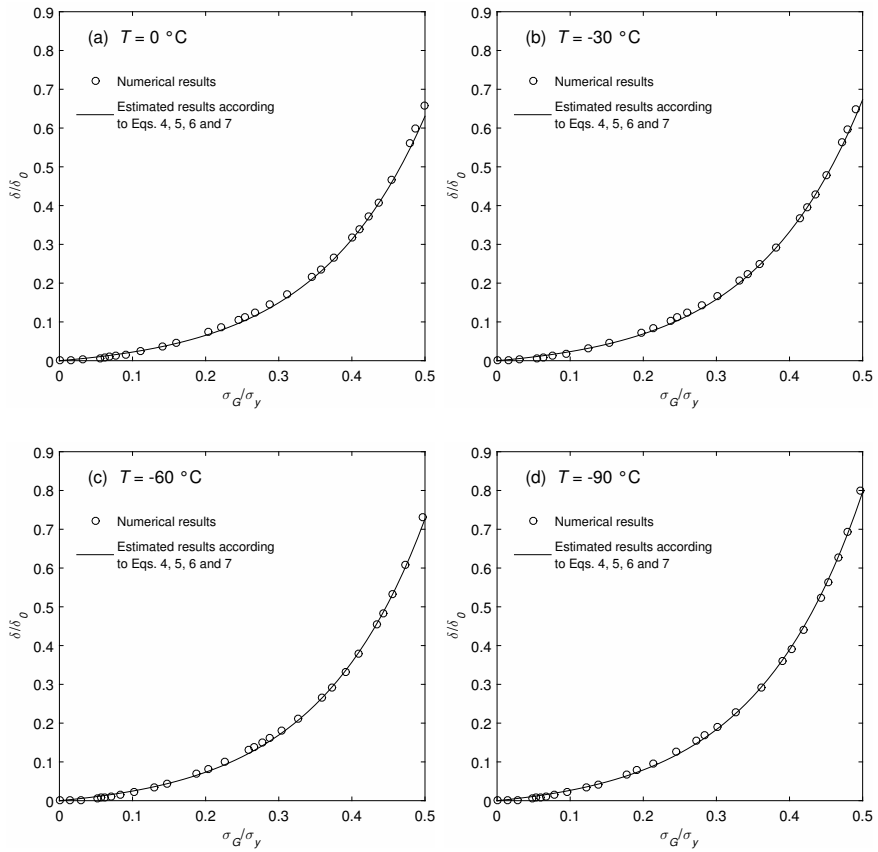


Figure 4.7: Proposed temperature dependent relation according to Eqs. 4.1, 4.2, 4.3 and 4.4 between CTOD and applied gross stress level in the SENT specimen compared to numerical results at (a) $0\text{ }^\circ\text{C}$, (b) $-30\text{ }^\circ\text{C}$, (c) $-60\text{ }^\circ\text{C}$ and (d) $-90\text{ }^\circ\text{C}$.

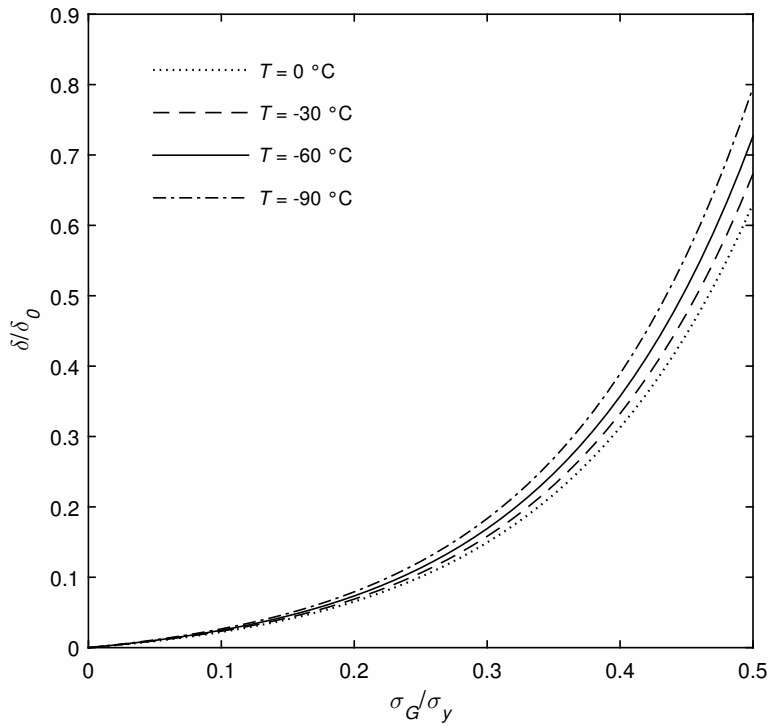


Figure 4.8: Comparison between CTOD curves estimated using the proposed CTOD model at four different temperatures.

behavior of the yield strength and Lüders strain to estimate the CTOD in a SENT specimen at different temperatures and gross stress levels. The model may also be modified to estimate the CTOD for other geometries, such as for cracks in pipelines in Arctic conditions. The model should also be sufficient to use for other similar materials if their tensile behavior is comparable and the effect of temperature on the tensile behavior is known.

4.4 Influence of crack depth on Lüders strain effect

The effect of crack depth, a/W , on the crack driving force is studied in the literature, but the influence of crack depth on the effect of Lüders strain on the crack driving force is not found in the literature. The proposed CTOD model can be modified to be used for varying crack depths if the effect of Lüders strain on CTOD is not changing behavior with the crack depth. The influence of crack depth is studied by using five similar FE models with a/W ranging from 0.1 to 0.5, as earlier shown in Figure 3.2. Analyses with these five models are performed with several materials displaying a series of varying Lüders strains and yield stresses to uncover differences from the earlier results. Yield strengths equal to 400 MPa and 700 MPa are used, while 0, 0.5 %, 1 %, 2 %, 3 %, 5 % and infinite Lüders strains are studied. The results are shown in Figures 4.9 and 4.10, where the CTOD is shown versus the gross stress level divided by $1 - a/W$, which is the same as the net section stress level in the crack ligament. The net section stress is defined as:

$$\sigma_N = \frac{\sigma_G}{1 - a/W} \quad (4.5)$$

The net section stress is used instead of gross stress to simplify the comparison between the results from analyses with different crack depths.

The results in Figures 4.9 and 4.10 show that there is a considerable effect of crack depth on CTOD, which also is expected and shown in literature. However, the effect of Lüders strain on the CTOD seems to be very similar for all the analysed crack depths. The influence of crack depth on the effect of Lüders strain on the crack driving force is hence negligible, and the proposed CTOD model can thus be modified to be used for varying a/W . This modification is not implemented in this work.

The proposed CTOD model is only valid for stress levels below yield stress in the crack ligament, and thus low CTOD values. Low CTOD values are relevant for Arctic applications, where many materials display low fracture toughness. It should however be noted that the crack depth has a significant influence on the effect of Lüders strain on the CTOD at very large global deformations outside the area of application for the proposed CTOD model. These effects can be investigated by plotting the CTOD versus the global strain of the specimen, which is done in Figures 4.11 and 4.12. The global strain of the specimen is defined as:

$$\varepsilon_G = \frac{\Delta L}{L_0} \quad (4.6)$$

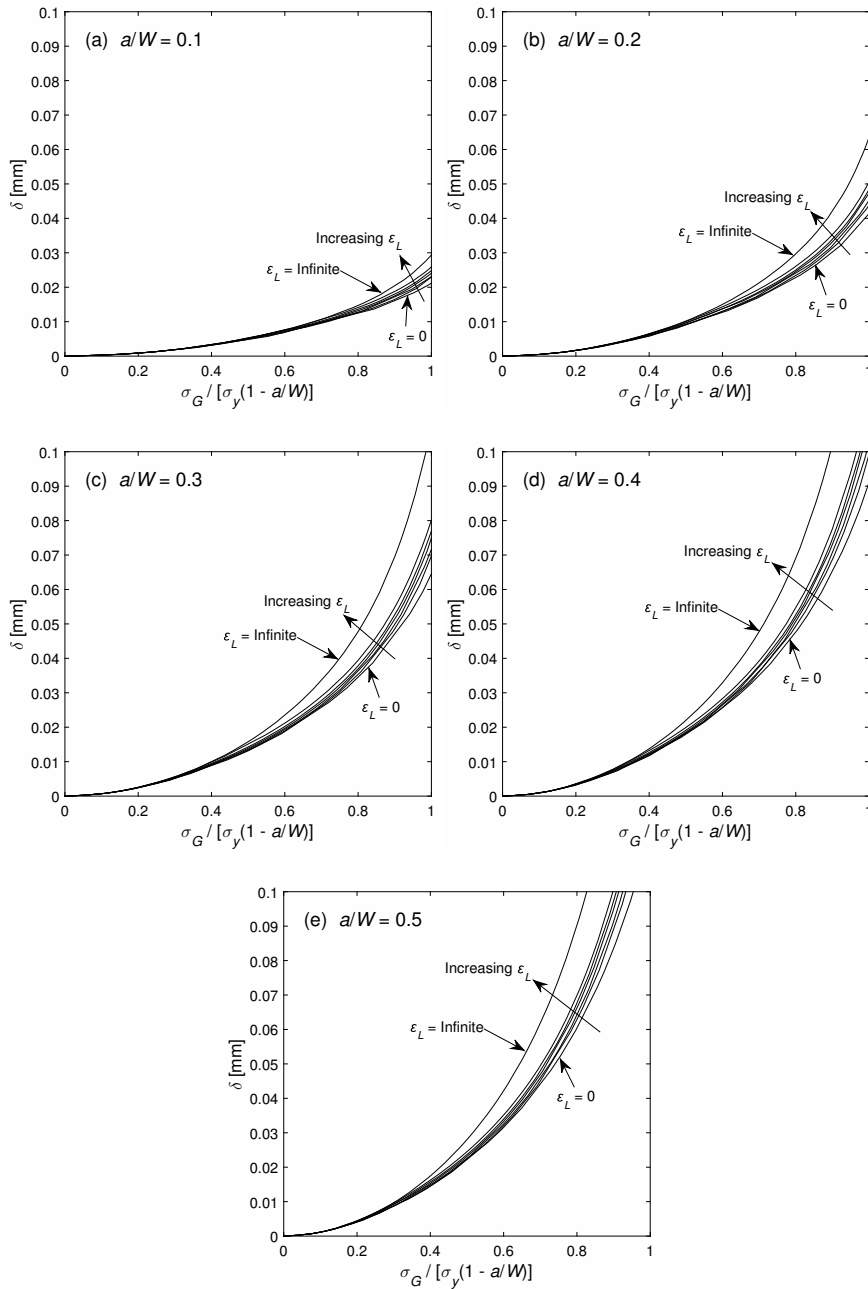


Figure 4.9: CTOD versus gross stress level divided by $1 - a/W$ with 0, 0.5%, 1%, 2%, 3%, 5% and infinite Lüders strains and a/W ranging from 0.1 to 0.5 in (a) to (e) respectively. The yield strength is 400 MPa.

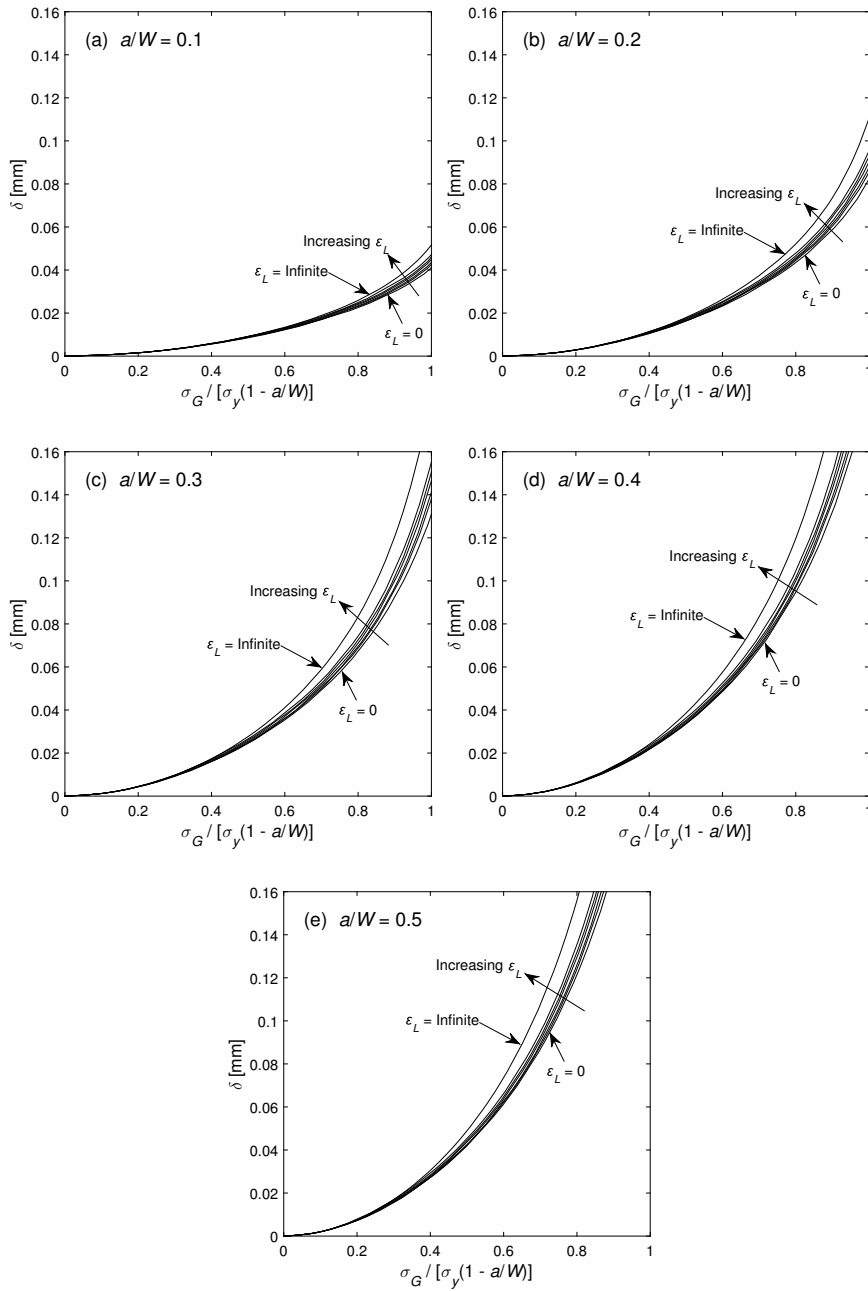


Figure 4.10: CTOD versus gross stress level divided by $1 - a/W$ with 0, 0.5%, 1%, 2%, 3%, 5% and infinite Lüders strains and a/W ranging from 0.1 to 0.5 in (a) to (e) respectively. The yield strength is 700 MPa.

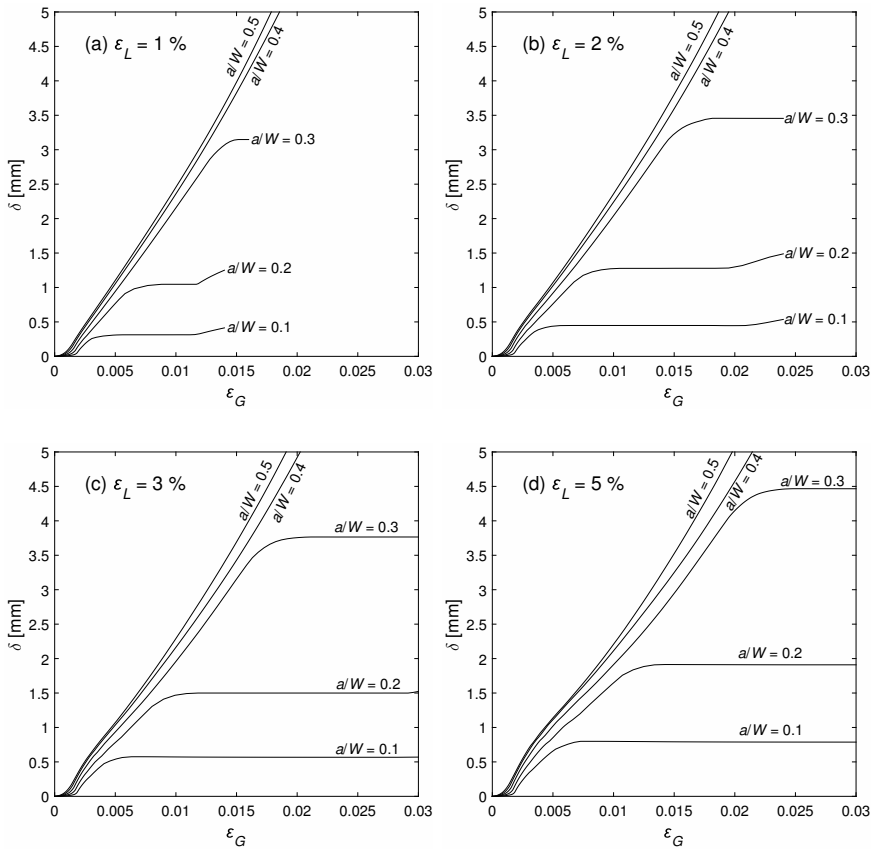


Figure 4.11: CTOD versus global strain with a/W ranging from 0.1 to 0.5 and 1% to 5% Lüders strain in (a) to (d) respectively. The yield strength is 400 MPa.

where ΔL is the tensile deformation of the specimen and L_0 is the initial specimen length.

Similar to the stress-strain curve for a material displaying Lüders or Lüders-like instabilities, some of the CTOD-strain curves in Figures 4.11 and 4.12 show similar kinds of horizontal Lüders plateaus. These Lüders plateaus occur when Lüders bands propagate in the uniform part of the specimen, which makes the stress and hence the CTOD remain approximately constant until the Lüders band has propagated through the entire specimen length. The Lüders plateau on the CTOD-strain curve is initiated when the crack tip plastic zone, which at this point has grown through the specimen to make a completely plastic crack ligament, has strain hardened to the point where the tension force is large enough to make the uniform part of the specimen reach the yield stress and Lüders instability. It should be noted that this behavior is taking place at very large deformation and thus very high CTOD values, which may be obtained only with very tough materials. The

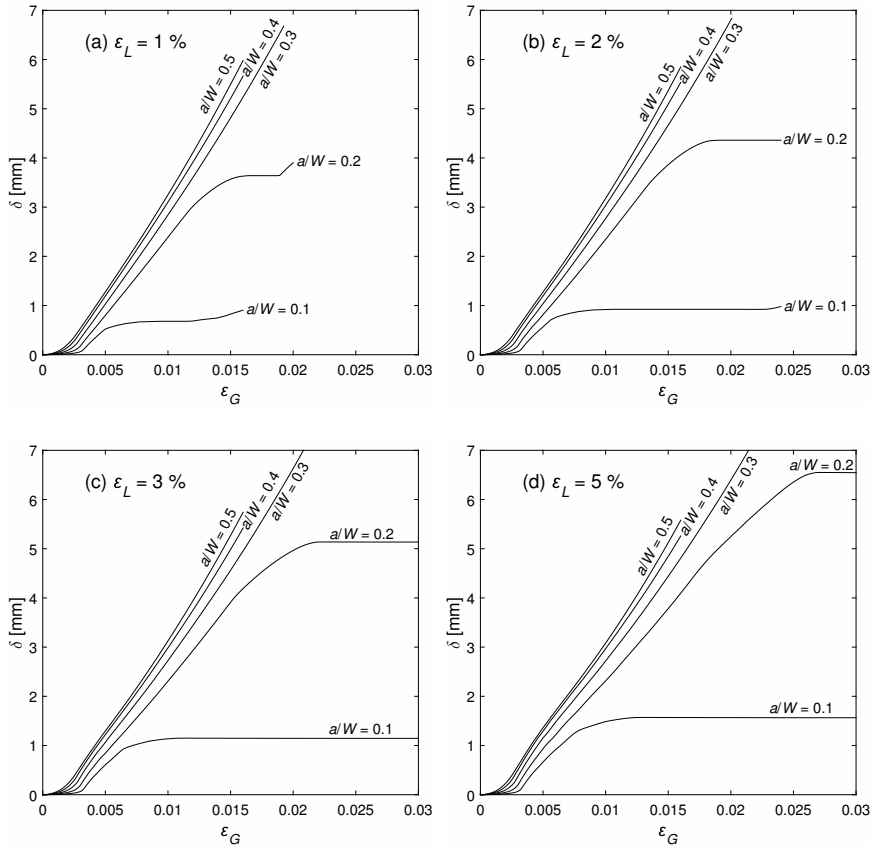


Figure 4.12: CTOD versus global strain with a/W ranging from 0.1 to 0.5 and 1% to 5% Lüders strain in (a) to (d) respectively. The yield strength is 700 MPa.

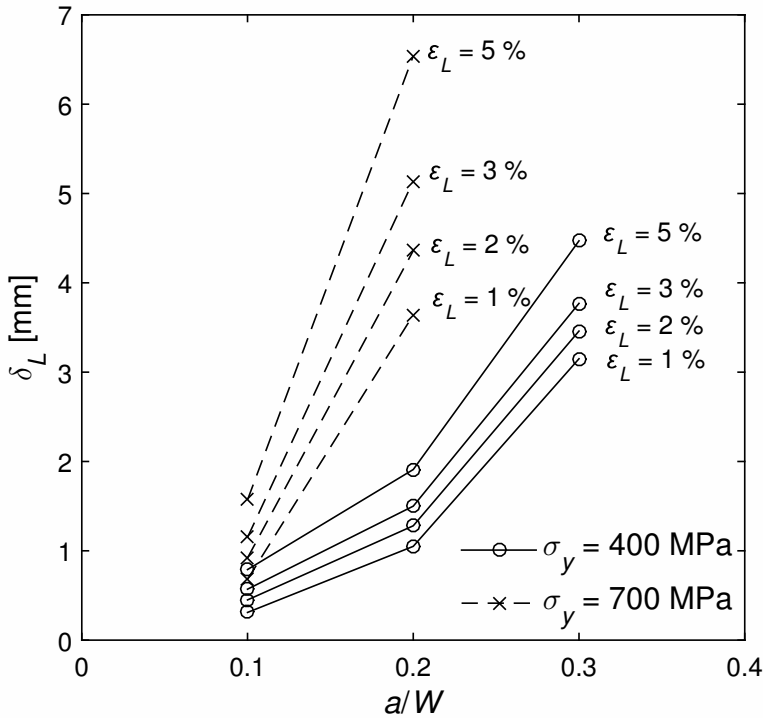


Figure 4.13: δ_L versus a/W using materials with four different Lüders strains and two yield strengths.

Lüders plateaus are only experienced for some of the crack depths as shown in Figures 4.11 and 4.12. This is due to necking happening in the crack ligament before the uniform Lüders behavior for deeper cracked specimens. The CTOD present when the uniform Lüders instability occurs as a Lüders plateau in the CTOD-strain curve is here denoted δ_L . The effects of a/W , σ_y and ε_L on δ_L are shown in Figure 4.13, where δ_L is shown as a function of crack depth for several materials with varying Lüders strain and yield strength.

As shown in Figure 4.13, δ_L increase with both a/W , σ_y and ε_L . They can all be expected to increase δ_L as they are all shown to increase the CTOD for given loadings and deformations, and hence increase δ at the point where uniform Lüders instabilities occur, where $\delta = \delta_L$.

4.5 Effects on the CMOD-CTOD relationship

The crack mouth opening displacement (CMOD) is very easy to measure experimentally and is thus often used directly to calculate the CTOD in fracture testing with single-edge-notched-bending (SENB) specimens. With SENT specimens this may not be as straightforward, but if the tensile properties of the material have

no or little effect on the CTOD-CMOD relationship, it should be possible to make equations that estimate the CTOD based on measuring just the CMOD, even if the yield strength and Lüders strain change, for instance due to testing at different temperatures. In Figure 4.14 several CTOD-CMOD results are shown, where δ is the CTOD and V is the CMOD. These are taken from the FE results shown earlier in this work, with 400 MPa and 700 MPa yield strength materials with Lüders strains equal to 0 and 2% for SENT specimens with a/W from 0.1 to 0.5. Because it is earlier shown that larger crack depth gives larger CTOD values (see Figures 4.9 and 4.10), a second pair of axes where the CTOD and CMOD are normalized by the crack depth a are added to facilitate comparison between the results in Figure 4.14.

The results show that the yield strength and Lüders strain have a significant effect on the CTOD-CMOD relationship. That effect is more evident at larger loads, as the difference between the curves increase with CTOD and CMOD. It is hence not straightforward to calculate the CTOD using the CMOD only, especially not when the tensile properties are changing, for instance due to changes in temperature. Increasing yield strength results in higher CTODs for given CMODs, while increasing Lüders strain results in lower CTODs. However, for $\delta/a < 0.03$ the differences are very small and may be neglected, and it is thus possible to use a simple CTOD-CMOD relation to calculate small CTODs.

It should also be noted that the curves are very similar when comparing the results from analyses with different a/W . This indicates that the crack depth has a very small effect on the relationship between δ/a and V/a , and it can probably be considered as insignificant when estimating the CTOD based on CMOD. It is hence possible to create functions for the relation between CTOD and CMOD that are dependent on the tensile properties of the material, but independent of the crack depth. For approximate estimates of the CTOD however, the results indicate that it is possible to use the measured CMOD directly without considering other parameters. For the range depicted in Figure 4.14 the CTOD can be roughly estimated as half the CMOD for all a/W between 0.1 and 0.5:

$$\delta_V = \frac{V}{2} \quad (4.7)$$

where δ_V is the approximate CTOD estimated using only the measured CMOD. It should be noted that this estimation might be very inaccurate, especially for large δ/a , and it should thus only be used as an indication of the real CTOD value.

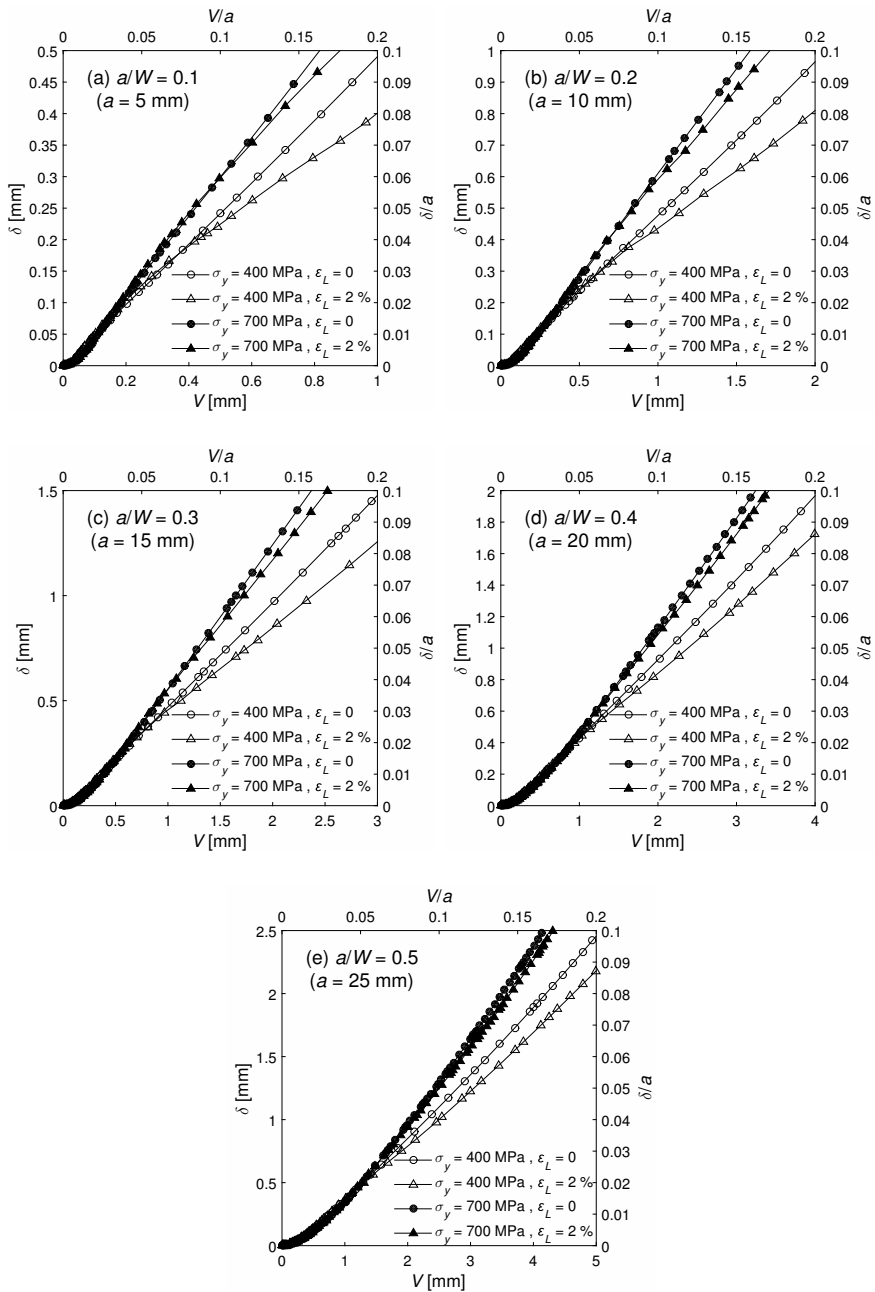


Figure 4.14: CTOD-CMOD results from FE analyses with 400 MPa and 700 MPa yield strength materials with Lüders strains equal to 0 and 2% and a/W ranging from 0.1 to 0.5 in (a) to (e) respectively. The top and rightmost axes are the CMOD and CTOD respectively normalized by the crack depth a to facilitate comparison between figures (a) to (f).

Conclusion

The effects of temperature dependent tensile properties on the crack driving force in a SENT specimen have been studied numerically, and an approximate model that predicts the CTOD based on tensile properties, temperature and loading is proposed. The material model is based on experimental results. The approximate CTOD model is based on a SENT specimen with crack depth $a/W = 0.5$, and the gross stress levels valid for the model are $\sigma_G/\sigma_y \leq 0.5$. The influence of a/W on the effect of Lüders strain on CTOD is additionally investigated, and the relation between CTOD and CMOD is studied.

The yield strength and Lüders strain are both usually increasing with decreasing temperature. In this work it is shown that increasing yield strength results in higher crack driving force in terms of CTOD for given gross stress levels. It is also shown that increasing Lüders strain results in higher CTOD. The crack driving force is thus increasing with decreasing temperature at given gross stress levels.

The proposed approximate CTOD model is based on the numerical results, and it is found to give quite accurate results when compared to numerical results using the same geometry, loading and material model as in this work. The model may also be modified to predict the CTOD for other similar geometries and materials at different temperatures. This can for instance make it useful in estimating the CTOD based on temperature and loading for a crack in a pipeline in Arctic conditions.

The crack depth has a considerable effect on the crack driving force, as expected, but the influence of a/W on the effect of Lüders strain on the CTOD is small. The proposed CTOD model can hence be modified to be valid for varying a/W between 0.1 and 0.5. This modification is not implemented in this work.

Additionally, plateaus similar to Lüders plateaus were found in several curves showing CTOD versus global specimen strain. This phenomenon happens when Lüders bands are propagating through the uniform part of the SENT specimen, and the CTOD is thus constant during that period ($\delta = \delta_L$). δ_L is found to increase with both yield strength, Lüders strain and crack depth.

Finally, a/W is found to have an almost insignificant effect on the relation between δ/a and V/a , while the yield strength and Lüders strain do both have a considerable influence on the CTOD-CMOD relation. It is thus not recommended to use the measured CMOD alone to estimate the CTOD, especially when the tensile properties are subject to change, for instance due to testing at different temperatures. It should however be possible to create functions that are dependent on tensile properties to estimate the CTOD based on CMOD measuring. It is also possible to roughly estimate the CTOD as half the CMOD for a/W from 0.1 to 0.5.

Bibliography

- Akselsen, O. M., Østby, E., Nyhus, B., 2012. Low temperature fracture toughness of X80 girth welds. In: The Twenty-second International Offshore and Polar Engineering Conference. International Society of Offshore and Polar Engineers, pp. 283–289.
- Akselsen, O. M., Østby, E., Thaulow, C., 2011. Low temperature toughness in SA welding of 420 MPa steel. In: The Twenty-first International Offshore and Polar Engineering Conference. International Society of Offshore and Polar Engineers, pp. 414–420.
- Baek, J.-H., Kim, Y.-P., Kim, W.-S., Kho, Y.-T., 2002. Effect of temperature on the charpy impact and CTOD values of type 304 stainless steel pipeline for LNG transmission. *KSME International Journal* 16 (8), 1064–1071.
- British Standards Institution, 2013. BS 7910: Guide to methods for assessing the acceptability of flaws in metallic structures.
- Costin, L. S., Duffy, J., 1979. The effect of loading rate and temperature on the initiation of fracture in a mild, rate-sensitive steel. *Journal of Engineering Materials and Technology* 101 (3), 258–264.
- Cottrell, A. H., Bilby, B. A., 1949. Dislocation theory of yielding and strain ageing of iron. *Proceedings of the Physical Society of London Section A* 62 (349), 49–62.
- Dahl, B. A., Ren, X. B., Akselsen, O. M., Nyhus, B., Zhang, Z. L., 2016. Effect of low temperature tensile properties on crack driving force for arctic applications. Submitted to international journal.
- Dassault Systèmes Simulia Corp., 2014. Abaqus 6.14.
- Det Norske Veritas, January 2006. Recommended practice DNV-RP-F108: Fracture control for pipeline installation methods introducing cyclic plastic strain.

-
- Eikrem, P. A., Zhang, Z. L., Nyhus, B., 2007. Effect of plastic prestrain on the crack tip constraint of pipeline steels. *International Journal of Pressure Vessels and Piping* 84 (12), 708–715.
- Eldin, A. S., Collins, S. C., 1951. Fracture and yield stress of 1020 steel at low temperatures. *Journal of Applied Physics* 22 (10), 1296.
- Gautier, D. L., Bird, K. J., Charpentier, R. R., Grantz, A., Houseknecht, D. W., Klett, T. R., Moore, T. E., Pitman, J. K., Schenk, C. J., Schuenemeyer, J. H., 2009. Assessment of undiscovered oil and gas in the Arctic. *Science* 324 (5931), 1175–1179.
- Hahn, G. T., 1962. A model for yielding with special reference to the yield-point phenomena of iron and related bcc metals. *Acta Metallurgica* 10 (8), 727–738.
- Hallai, J. F., Kyriakides, S., 2013. Underlying material response for Lüders-like instabilities. *International Journal of Plasticity* 47, 1–12.
- Heier, E., Østby, E., Akselsen, O. M., 2013. Reeling installation of rigid steel pipelines at low temperature. In: *The Twenty-third International Offshore and Polar Engineering Conference*. International Society of Offshore and Polar Engineers, pp. 265–269.
- Johnson, D. H., 2013. Lüders bands in RPV steel. PhD thesis, Cranfield University.
- Liu, J., Zhang, Z. L., Nyhus, B., 2008. Residual stress induced crack tip constraint. *Engineering Fracture Mechanics* 75 (14), 4151–4166.
- Liu, Y., Kyriakides, S., Hallai, J. F., 2015. Reeling of pipe with Lüders bands. *International Journal of Solids and Structures* 72, 11–25.
- Marais, A., Mazière, M., Forest, S., Parrot, A., Le Delliou, P., 2012. Identification of a strain-aging model accounting for Lüders behavior in a C-Mn steel. *Philosophical Magazine* 92 (28-30), 3589–3617.
- Mazière, M., Forest, S., 2013. Strain gradient plasticity modeling and finite element simulation of Lüders band formation and propagation. *Continuum Mechanics and Thermodynamics* 27 (1-2), 83–104.
- Nyhus, B., Polanco, M. L., Ørjasæter, O., 2003. SENT specimens an alternative to SENB specimens for fracture mechanics testing of pipelines. In: *ASME 2003 22nd International Conference on Offshore Mechanics and Arctic Engineering*. American Society of Mechanical Engineers, pp. 259–266.
- Ren, X., Nordhagen, H. O., Zhang, Z., Akselsen, O. M., 2015. Tensile properties of 420 MPa steel at low temperature. In: *The Twenty-fifth International Offshore and Polar Engineering Conference*. International Society of Offshore and Polar Engineers, pp. 346–352.

-
- Ritchie, R. O., Knott, J. F., Rice, J. R., 1973. On the relationship between critical tensile stress and fracture toughness in mild steel. *Journal of the Mechanics and Physics of Solids* 21 (6), 395–410.
- Robertson, C. F., Obrtlík, K., Marini, B., 2007. Dislocation structures in 16MND5 pressure vessel steel strained in uniaxial tension at different temperatures from -196°C up to 25°C . *Journal of Nuclear Materials* 366 (1-2), 58–69.
- Shioya, T., Shioiri, J., 1976. Elastic-plastic analysis of the yield process in mild steel. *Journal of the Mechanics and Physics of Solids* 24 (4), 187–204.
- Sieurin, H., Sandström, R., 2006. Fracture toughness of a welded duplex stainless steel. *Engineering Fracture Mechanics* 73 (4), 377–390.
- Sorem, W. A., Dodds Jr, R. H., Rolfe, S. T., 1991. Effects of crack depth on elastic-plastic fracture toughness. *International Journal of Fracture* 47 (2), 105–126.
- Standard Norge, 2008. NORSOK M-120: Material data sheets for structural steels.
- Thaulow, C., Østby, E., Nyhus, B., Zhang, Z. L., Skallerud, B., 2004. Constraint correction of high strength steel: Selection of test specimens and application of direct calculations. *Engineering Fracture Mechanics* 71 (16-17), 2417–2433.
- Tsuchida, N., Tomota, Y., Nagai, K., Fukaura, K., 2006. A simple relationship between Lüders elongation and work-hardening rate at lower yield stress. *Scripta Materialia* 54 (1), 57–60.
- Tsukahara, H., Iung, T., 1998. Finite element simulation of the Piobert–Lüders behavior in an uniaxial tensile test. *Materials Science and Engineering: A* 248 (1–2), 304–308.
- Wenman, M. R., Chard-Tuckey, P. R., 2010. Modelling and experimental characterisation of the Lüders strain in complex loaded ferritic steel compact tension specimens. *International Journal of Plasticity* 26 (7), 1013–1028.
- Wilson, M. L., Hawley, R. H., Duffy, J., 1980. The effect of loading rate and temperature on fracture initiation in 1020 hot-rolled steel. *Engineering Fracture Mechanics* 13 (2), 371–385.
- Xu, J., Zhang, Z. L., Østby, E., Nyhus, B., Sun, D. B., 2009. Effects of crack depth and specimen size on ductile crack growth of SENT and SENB specimens for fracture mechanics evaluation of pipeline steels. *International Journal of Pressure Vessels and Piping* 86 (12), 787–797.
- Xu, J., Zhang, Z. L., Østby, E., Nyhus, B., Sun, D. B., 2010. Constraint effect on the ductile crack growth resistance of circumferentially cracked pipes. *Engineering Fracture Mechanics* 77 (4), 671–684.

-
- Zerbst, U., Ainsworth, R. A., Beier, H. T., Pisarski, H., Zhang, Z. L., Nikbin, K., Nitschke-Pagel, T., Munstermann, S., Kucharczyk, P., Klingbeil, D., 2014. Review on fracture and crack propagation in weldments - a fracture mechanics perspective. *Engineering Fracture Mechanics* 132, 200–276.
- Zhang, Y. T., Qiao, J. L., Ao, T., 2007. Strain softening of materials and Lüders-type deformations. *Modelling and Simulation in Materials Science and Engineering* 15 (2), 147–156.
- Østby, E., Akselsen, O. M., Hauge, M., Horn, A. M., 2013. Fracture mechanics design criteria for low temperature applications of steel weldments. In: *The Twenty-third International Offshore and Polar Engineering Conference*. International Society of Offshore and Polar Engineers, pp. 315–321.

Appendix

Master thesis contract

The signed master thesis contract document with the problem text is attached on the next pages.

**MASTER THESIS SPRING 2016
FOR
STUD.TECHN. BJØRN AUGDAL DAHL**

Effects of low temperature tensile properties on crack driving force for Arctic applications

Virkninger av mekaniske egenskaper ved lav temperatur på drivende kraft for sprekkvekst for arktiske anvendelser

In exploration of oil and gas in the arctic region, the low ambient temperature may be the major challenge for structural materials. This is due to the ductile-to-brittle transition (DBT) taking place at a certain temperature below 0°C. Design temperatures down to -60°C may be required in the worst case. Previous investigations have shown that the properties of weldments of available structural steels, including both the heat affected zone (HAZ) and the weld metal, are insufficient or on the borderline for arctic application down to -60°C, and may thus not give the required robust solutions. The present work is initiated to establish better understanding how stress-strain behaviour changes with temperature from room temperature and down to -60°C, and how this influence the crack driving force and toughness. Numerical simulations will be used extensively for this purpose.

The topics to be investigated will be:

- Effect of temperature on stress-strain behaviour for different structural steels
- Effect of temperature on Lüder strain
- Effect of temperature on yield to tensile ratio (work hardening ability)
- Effect of temperature on the fracture resistance/crack driving force

Most work is supposed to be performed through the use of finite element modelling, but the candidate will have access to all test results in the Arctic Materials projects.

Formal requirements:

Three weeks after start of the thesis work, an A3 sheet illustrating the work is to be handed in. A template for this presentation is available on the IPM's web site under the menu "Masteroppgave" (<https://www.ntnu.no/web/ipm/masteroppgave-ved-ipm>). This sheet should be updated one week before the master's thesis is submitted.

Risk assessment of experimental activities shall always be performed. Experimental work defined in the problem description shall be planned and risk assessed up-front and within 3 weeks after receiving the problem text. Any specific experimental activities which are not properly covered by the general risk assessment shall be particularly assessed before

performing the experimental work. Risk assessments should be signed by the supervisor and copies shall be included in the appendix of the thesis.

The thesis should include the signed problem text, and be written as a research report with summary both in English and Norwegian, conclusion, literature references, table of contents, etc. During preparation of the text, the candidate should make efforts to create a well arranged and well written report. To ease the evaluation of the thesis, it is important to cross-reference text, tables and figures. For evaluation of the work a thorough discussion of results is appreciated.

The thesis shall be submitted electronically via DAIM, NTNU's system for Digital Archiving and Submission of Master's theses.

The contact person is [navn på veileder i utlandet, bedrift eller lignende].


for Torgeir Welo
Head of Division


Odd M. Akselsen
Professor/Supervisor

 **NTNU**
Norges teknisk-
naturvitenskapelige universitet
Institutt for produktutvikling
og materialer

Risk assessment

The mandatory risk assessment for the master thesis work is attached on the next pages.

NTNU	Utarbeidd av	Nummer	Dato
	HMS-avd.	HMSRV2601	22.03.2011
HMS	Godkjent av		Etabler
	Faktor		01.12.2006

Kartlegging av risikofylt aktivitet

Enhet:

Dato: 03.02.16

Linjeleder:

Deltakere ved kartleggingen (m/ funksjon): Bjørn Augdal Dahl (student), Odd Magne Akselsen (ansv. veileder)

(Ansv. veileder, student, evt. medveiledere, evt. andre m. kompetanse)

Kort beskrivelse av hovedaktivitet/hovedprosess:

Masteroppgave Bjørn Augdal Dahl, IPM, NTNU, SINTEF. Effect of Low Temperature Tensile Properties on Crack Driving Force for Arctic applications.

Er oppgaven rent teoretisk? (JA/NEI): JA

«JA» betyr at veileder innestår for at oppgaven ikke inneholder noen aktiviteter som krever risikovurdering. Dersom «JA»: Beskriv kort aktiviteten i kartleggingskjemaet under. Risikovurdering trenger ikke å fylles ut.

Signaturer:

Ansvarlig veileder: 

Student: 

ID nr.	Aktivitet/prosess	Ansvarlig	Eksisterende dokumentasjon	Eksisterende sikringstiltak	Lov, forskrift o.l.	Kommentar
	Numeriske analyser på datamaskin					

NTNU		Utarbeidet av	Nummer	Dato
		HMS-avd.	HMSFRV2601	22.03.2011
HMS	Risikovurdering	Godkjent av		Erstatler
		Rektor		01.12.2006
				

Dato:

Enhet:

Linjeleder:

Deltaere ved kartleggingen (m/ funksjon):

(Ansv. Veileder, student, evt. medveileder, evt. andre m. kompetanse)

Risikovurderingen gjelder hovedaktivitet: Masteroppgave student xx. Tittel på oppgaven.

Signaturer: Ansvarlig veileder:

Student:

ID nr	Aktivitet fra kartleggings-skjemaet	Mulig uønsket hendelse/ belastning	Vurdering av sannsynlighet (1-5)	Vurdering av konsekvens:				Risiko-Verdi (menneske)	Kommentarer/status Forslag til tiltak
				Menneske (A-E)	Ytre miljø (A-E)	ØK/ materiell (A-E)	Om-dømme (A-E)		

NTNU		Utarbeidet av	Nummer	Dato
HMS		HMS-avd.	HMSRV2601	22.03.2011
Risikovurdering		Godkjent av	Eriater	
		Faktor		01.12.2006
				

Sannsynlighet vurderes etter følgende kriterier:

Svært liten 1	Liten 2	Middels 3	Stor 4	Svært stor 5
1 gang pr 50 år eller sjeldnere	1 gang pr 10 år eller sjeldnere	1 gang pr år eller sjeldnere	1 gang pr måned eller sjeldnere	Slyr ukentlig

Konsekvens vurderes etter følgende kriterier:

Gradering	Menneske	Ytre miljø Vann, jord og luft	Øivmaterieell	Omdømme
E Svært Alvorlig	Død	Svært langvarig og ikke reversibel skade	Drifts- eller aktivitetssjans > 1 år.	Troverdighet og respekt betydelig og varig svekket
D Alvorlig	Alvorlig personskade. Mulig uførlighet.	Langvarig skade. Lang restitusjonstid	Drifts- eller aktivitetssjans > ½ år	Troverdighet og respekt betydelig svekket
C Moderat	Alvorlig personskade.	Mindre skade og lang restitusjonstid	Drifts- eller aktivitetssjans < 1 mnd	Troverdighet og respekt svekket
B Liten	Skade som krever medisinsk behandling	Mindre skade og kort restitusjonstid	Drifts- eller aktivitetssjans < 1uke	Negativ påvirkning på troverdighet og respekt
A Svært liten	Skade som krever førstehjelp	Ubetydelig skade og kort restitusjonstid	Drifts- eller aktivitetssjans < 1dag	Liten påvirkning på troverdighet og respekt

Risikoverdi = Sannsynlighet x Konsekvens

Beregn risikoverdi for Menneske. Enheten vurderer selv om de i tillegg vil beregne risikoverdi for Ytre miljø, Økonomi/materieell og Omdømme. I så fall beregnes disse hver for seg.

Til kolonnen "Kommentarer/status, forslag til forebyggende og korrigerende tiltak":

Tiltak kan påvirke både sannsynlighet og konsekvens. Prioriter tiltak som kan forhindre at hendelsen inntreffer, dvs. sannsynlighetsreduserende tiltak foran skjerpet beredskap, dvs. konsekvensreduserende tiltak.

NTNU		Fisikomatrise		Utarbeidet av	Nummer	Dato
				HMS-avd.	HMSRFV2604	08.03.2010
HMS/KS				godkjent av		Erstatler
				Rektor		09.02.2010
						

KONSEKVENNS					
Svært alvorlig	E1	E2	E3	E4	E5
Alvorlig	D1	D2	D3	D4	D5
Moderat	C1	C2	C3	C4	C5
Liten	B1	B2	B3	B4	B5
Svært liten	A1	A2	A3	A4	A5
	Svært liten	Liten	Middels	Stor	Svært stor
SANNSYNLIGHET					

Prinsipp over akseptkriterium. Forklaring av fargene som er brukt i risikomatrisen.

Farge	Beskrivelse
Rød	Uakseptabel risiko. Tiltak skal gjennomføres for å redusere risikoen.
Gul	Vurderingsområde. Tiltak skal vurderes.
Grønn	Akseptabel risiko. Tiltak kan vurderes ut fra andre hensyn.

Effect of low temperature tensile properties on crack driving force for Arctic applications

A large part of this work is based on Dahl et al. (2016), which is written during the project and Master's thesis period. The paper was submitted to an international journal in May 2016. The current revision of the paper is attached on the next pages.

Effect of low temperature tensile properties on crack driving force for Arctic applications

B.A. Dahl^a, X.B. Ren^b, O.M. Akselsen^{a,b}, B. Nyhus^b, Z.L. Zhang^{c,*}

^a*Department of Engineering Design and Materials, NTNU, N-7491, Trondheim, Norway*

^b*SINTEF Materials and Chemistry, N-7465, Trondheim, Norway*

^c*Department of Structural Engineering, NTNU, N-7491, Trondheim, Norway*

Abstract

Many petroleum companies expand their activities further north towards the Arctic region, resulting in design temperatures down to $-60\text{ }^{\circ}\text{C}$, which is much lower than what is usual for most current petroleum installations. As properties of steels are temperature dependent, it is of great interest to evaluate the effects of low temperature on the crack driving force in steels. The present work investigates these effects numerically using a finite element model of a single-edge-notched-tension (SENT) specimen with crack depth $a/W = 0.5$. The effects of Lüders strain and yield strength are studied for gross stress levels $\sigma_G/\sigma_y \leq 0.5$, and it is shown that an increase in yield strength and Lüders strain, as a result of Arctic temperature, enhances the crack driving force. An approximate model that can be used to estimate the crack driving force based on yield strength, Lüders strain and loading is proposed.

Keywords: Arctic materials, crack driving force, Lüders plateau, low temperature, tensile properties

1. Introduction

The exploitation of hydrocarbons is continuously moving into new areas and harsher environments. Many petroleum companies are expanding their activities further north, where a considerable part of the undiscovered oil and gas resources is expected to exist [1]. Consequently the structures built must be able to withstand the low temperatures present in the Arctic climate. Most structural materials have different behavior in such low temperatures, and this must be accounted for when designing and constructing structures to avoid accidents related to structural failure.

Much research has been carried out to study the behavior of steels in changing temperatures. The most obvious temperature dependent parameter is the yield strength, which for most steels increase with decreasing temperature [2–14]. Another temperature dependent property is the ductile-to-brittle transition (DBT) in steels. Due to the DBT, many steels become brittle when the temperature is sufficiently decreased, but the DBT is however not in the scope of this study.

Many steels, and also other materials, experience so-called Lüders and Lüders-like instabilities. These instabilities are associated with unpinning of dislocations from nitrogen and carbon atmospheres and dislocation multiplication, and they result in macroscopic inhomogeneous deformation [8, 15–20]. The Lüders instability is in uniaxial tensile tests observed as nearly horizontal stress plateaus, called Lüders plateaus, in the stress-strain curves after reaching the elastic limit of the material. This instability can be physically observed as localized deformation bands, called Lüders bands, propagating on the surface of uniaxial tensile tests. Structural steels often show this behavior. The amount of plastic straining occurring due to the Lüders instability is often called Lüders strain. Studies have shown that the Lüders strain is both

*Corresponding author

Email address: zhiliang.zhang@ntnu.no (Z.L. Zhang)

rate and temperature dependent, and decreasing temperature is often associated with larger Lüders strain [7–9, 18, 21].

The fracture toughness of a material is often measured by using fracture mechanics tests, and is described by a single parameter, such as a critical stress intensity factor (K), crack tip opening displacement (CTOD, δ) or J -integral, depending on if it is a linear elastic or elastoplastic dominated fracture. The fracture toughness of steels is usually reduced when decreasing the temperature [5, 10, 12–14, 22].

The fracture toughness can be interpreted as a measure of the ability of a material to resist fracture, while the crack driving force, on the other hand, can be defined as the force which opens the crack. The fracture toughness can be regarded as the critical level of crack driving force, and the same way as a critical CTOD can be a measure of the fracture toughness, the CTOD is often used as a measure of the crack driving force which changes with loading. Due to temperature dependent material parameters, decreasing temperature is assumed to have an effect on the crack driving force [23]. The goal of this work is hence to study the effect of low temperature material properties of steels, as expected in Arctic applications, on the crack driving force by performing finite element analyses. This effect is studied by simulating fracture tests of a single-edge-notched-tension (SENT) specimen with a material model where the temperature dependent material parameters can be changed. The CTOD is used as a measure of the crack driving force. A SENT specimen is studied because it is used as a fracture specimen to estimate fracture toughness of steels used for pipeline applications where other specimen types give unnecessarily conservative results, such as for girth welds in pipes [24, 25].

The results will be utilized to propose approximate CTOD models that can be used to estimate the crack driving force in a SENT specimen at low temperatures by using only tensile properties of the material. This can for instance also be useful for estimating the CTOD or maximum stress allowed in a cracked pipeline in Arctic climate.

2. Experimental work on low temperature tensile properties

The recent work by Ren et al. [9] and Østby et al. [23] has presented tensile properties of a 420 MPa steel at different temperatures ranging from 0 °C down to –90 °C. They tested both base material, weld metal and weld thermal simulated microstructure of steel. Smooth round specimens with gauge diameters between 10 mm and 12 mm were used for testing the base material, and they were loaded with a strain rate of $8 \times 10^{-4} \text{ s}^{-1}$. An example of engineering stress-strain results is shown in Fig. 1.

The results in Fig. 1 show that both the yield strength and the Lüders strain increase with decreasing temperature. The yield strength and Lüders strain from 0 °C to –90 °C are ranging from approximate 470 MPa and 1.4 % to 540 MPa and 2.2 % respectively.

Tensile properties at low temperatures cannot always be obtained due to cost or practical reasons, and several corrections for calculating tensile properties at temperatures lower than room temperature are thus proposed in literature [9, 23, 26].

Ren et al. [9] introduced a modified version of the correction proposed by Østby et al. [26] based on their results from tensile tests on a 420 MPa steel:

$$\sigma_{y,T} = 420 \text{ MPa} + 0.73 \text{ MPa} \left(\frac{10^5}{491 + 1.8T} - 137 \right) \quad (1)$$

where $\sigma_{y,T}$ is the yield strength in MPa at temperature T in °C. They proposed in addition a relation between Lüders strain and temperature:

$$\varepsilon_L = 0.0142 \exp(-0.005T) \quad (2)$$

where T is the temperature in °C and ε_L is the Lüders strain. Eqs. 1 and 2 are expected to be valid for the tested temperature range from –90 °C to 0 °C. The effect of the low temperature tensile properties on the crack driving force will be numerically studied in the following, where Eqs. 1 and 2 will be used to estimate the yield strength and Lüders strain present at different temperatures.

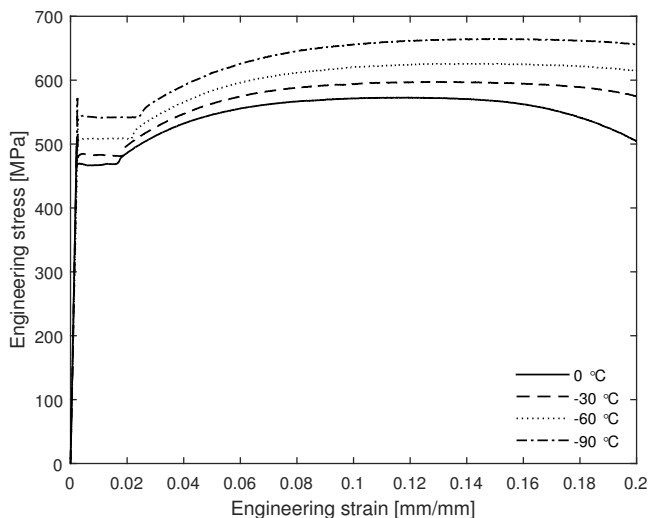


Fig. 1. Engineering stress-strain curves of a 420 MPa steel at different temperatures. Taken from [9].

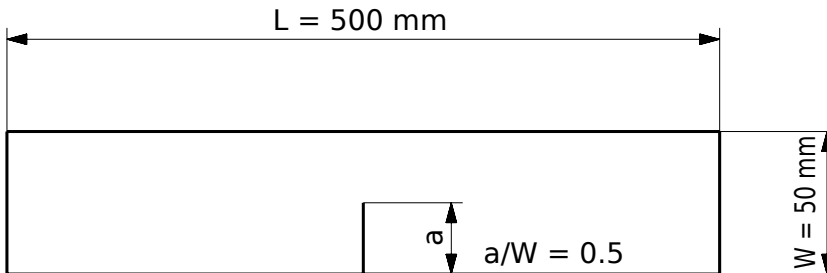


Fig. 2. Illustration of a SENT specimen with dimensions.

3. Material model and numerical procedure

The numerical simulations were performed using the commercial finite element program Abaqus 6.14 [27]. The finite element (FE) model studied is a two-dimensional plane strain SENT specimen. The symmetry is utilized by modelling only half of the specimen. The width of the specimen is 50 mm, and the other dimensions are determined using a recommended practice [25]: $L/W = 10$ and $a/W = 0.5$, where W is the specimen width, L is the specimen length, and a is the crack length as illustrated in Fig. 2.

Large plastic deformations are expected at the crack tip, and the crack is modelled as an initially blunted crack with a tip radius of 10 μm . The large-displacement formulation that accounts for nonlinear geometric effects (NLGEOM) is used in the analyses. The finite element mesh consists of 1355 8-node plane strain CPE8 elements. The mesh is refined around the crack tip where large strain gradients are expected, which is the primary area of interest in this study. There are 10 elements along the edge of the crack tip. The mesh and crack tip radius were determined based on a convergence study with varying mesh densities, element types and crack tip radii. The final finite element mesh is shown in Fig. 3.

A uniform displacement is applied on the end of the half specimen to simulate the tension of a clamped SENT specimen. The displacement is set as high as needed to make the ligament net section stress exceed

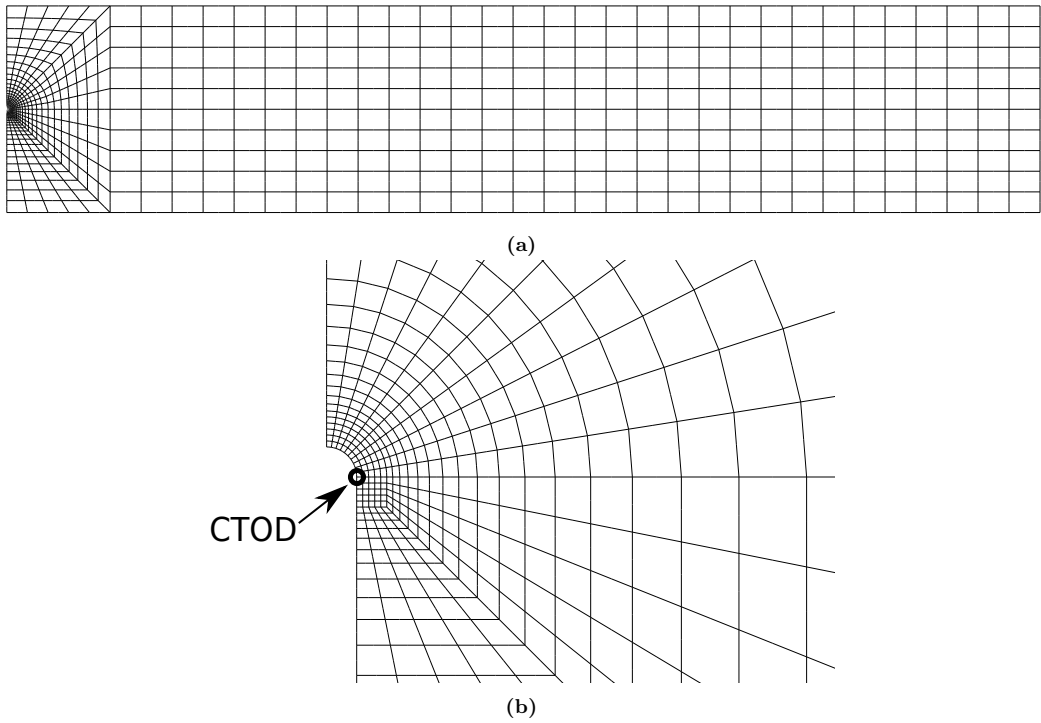


Fig. 3. (a) Global and (b) local finite element mesh. The node where CTOD is measured is marked by the circle in (b).

Table 1
Constant material parameters.

E	ν	K	n
210 GPa	0.3	685 MPa	0.576

the yield stress of the material.

An elastoplastic material model based on uniaxial tensile tests of the steel in [9] is used in the analyses. The material displays isotropic linear elasticity and J_2 -plasticity with isotropic hardening, while an amount of Lüders straining is added in the transition between the elastic and plastic behavior. The Lüders behavior is modelled as a simplified horizontal Lüders plateau in the plastic stress-strain curve. There are many proposals for more realistic modelling of the Lüders instability in literature, which for instance include strain drops or strain softening [8, 17, 19, 20, 28–31], but the simplified flat Lüders plateau is assumed to give a sufficient approximation to the material behavior in the present analysis. This is verified by doing analyses using a material model similar to the model in [20]. The modelled stress-strain curve is fitted to true stress-strain data from the uniaxial tensile tests in [9], and it is then modified to create several similar materials with varying parameters such as yield stress and Lüders strain. The material can be described by

$$\sigma = \begin{cases} E\varepsilon & \text{if } 0 \leq \varepsilon < \frac{\sigma_y}{E} \\ \sigma_y & \text{if } \frac{\sigma_y}{E} \leq \varepsilon < \frac{\sigma_y}{E} + \varepsilon_L \\ \sigma_y + K \left(\varepsilon - \left(\frac{\sigma_y}{E} + \varepsilon_L \right) \right)^n & \text{if } \varepsilon \geq \frac{\sigma_y}{E} + \varepsilon_L \end{cases} \quad (3)$$

in uniaxial tension, where σ is the uniaxial stress, E is the Young’s modulus, ε is the uniaxial strain, σ_y is the yield stress, ε_L is the Lüders strain, K is a strength coefficient and n is the strain hardening exponent. For loads and deformations in the two-dimensional plane, the Poisson’s ratio ν is also needed. The yield stress and Lüders strain are the temperature dependent parameters to be studied. The constant material parameters are summarized in Table 1, where K and n are determined by fitting Eq. 3 to the true stress-strain data from the uniaxial tensile testing in [9]. Eq. 3 divides the stress-strain curve into three parts: the linear elastic part, Lüders plateau and plastic hardening, as illustrated in Fig. 4. As only quasi-static simulations are performed, there are no rate dependencies in the material model.

4. Results and discussion

To study how temperature dependent material properties affect the crack driving force, different analyses were performed where the parameters of interest were studied individually, and thereafter their combined effect was investigated. This study focuses on the effects of varying yield strength and Lüders strain on the CTOD. The CTOD is measured as twice the opening displacement of the fixed node in the transition point between the semicircular crack tip edge and the straight crack surface, as shown by the circle in Fig. 3b, which is equivalent to the initially 90 degree intercept method. The same procedure using a fixed node to calculate CTOD has been utilized in [32–36]. The results will be used to propose approximate CTOD models that can be utilized to estimate the CTOD based on given loadings and temperatures.

4.1. Effect of yield stress

The effect of yield stress was studied by keeping the other parameters constant. Analyses with different yield stresses were performed with different levels of Lüders strain. A total of 36 analyses were performed to produce the following results, where 6 different yield stress levels, 300, 400, 500, 600, 700 and 800 MPa, were tested with 6 different levels of Lüders strain ranging from 0 to infinite. Examples of plastic uniaxial material responses are shown in Fig. 5, where four materials with 400, 500, 600 and 700 MPa yield strength and 0, 1%, 3% and infinite Lüders strain respectively are displayed.

The CTOD results are plotted versus the gross stress level in each case in Fig. 6. The gross stress level is defined as σ_G/σ_y , where σ_G is the gross stress defined as $\sigma_G = F_{\parallel}/(Wt)$, where F_{\parallel} is the longitudinal

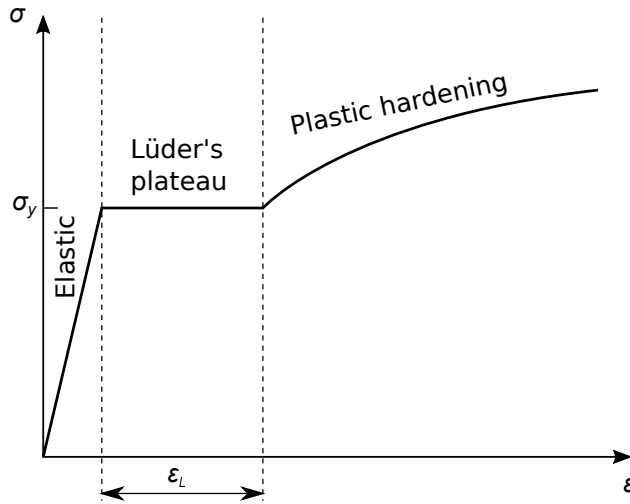


Fig. 4. Illustration of a material model showing the three different parts of the stress-strain curve.

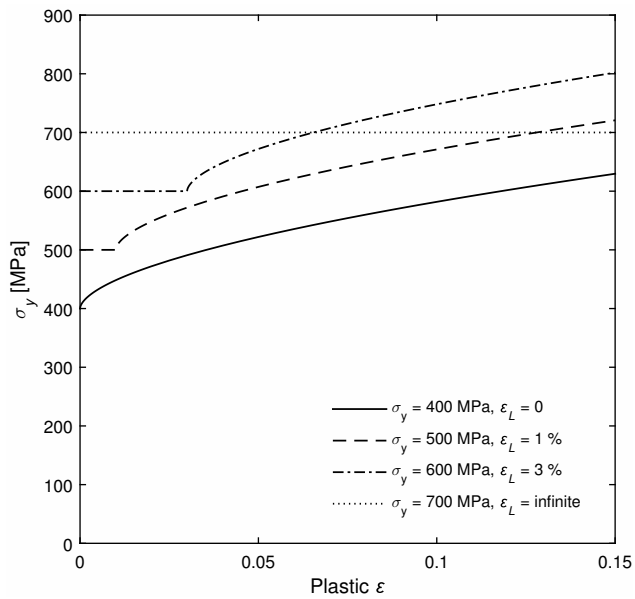


Fig. 5. Examples of some of the model materials studied.

reaction forces at the specimen end, W is the specimen width and t is the specimen thickness. These results show that increasing yield stress results in increased CTOD at the same σ_G/σ_y . This can be expected as the same relative stress level corresponds to higher stresses and thus higher elastic strains in materials with higher yield strengths. This leads to a larger elastic deformation and hence a larger CTOD at the same relative stress level for a material with higher yield stress.

4.2. Effect of Lüders strain

The effect of the temperature dependent Lüders strain was studied by changing the amount of Lüders strain in the material model, while keeping the other parameters constant. This is the same as changing the length of the Lüders plateau in the uniaxial stress-strain curve. A total of 36 analyses were performed to produce the following results, where 6 different Lüders strains, 0, 1, 2, 3, 5% and infinite, were tested with 6 different levels of yield stress ranging from 300 to 800 MPa.

The results from the simulations are shown in Fig. 7, where the CTOD is plotted against the gross stress level. These are the same results as in Fig. 6, but rearranged so that the effect of Lüders strain can be more easily studied. The results indicate that increasing Lüders strain, for instance caused by decreasing temperature, yields a larger CTOD, and hence a larger crack driving force, for a given loading. This can be explained due to the larger plastic deformation allowed by a material with larger Lüders strain. Fig. 7 also indicates that the effect of Lüders strain on the CTOD is more evident at larger stress levels due to the difference in allowed plastic deformation. It should also be noted that the effect approaches a maximum for very large Lüders strains, as the curves approach the one for the material with infinite Lüders strain. The material with infinite Lüders strain corresponds to a material which displays perfect plasticity.

4.3. Approximate CTOD model

The results from the previous sections clearly show that the tensile properties have an effect on the crack driving force. These results will be utilized to create an approximate model that can be used for estimating the crack driving force in terms of CTOD based on yield strength and Lüders strain. This model will later in this section be coupled to the effect of temperature on the yield strength and Lüders strain according to Eqs. 1 and 2. The model can thus be used to estimate the CTOD in a SENT specimen based on loading and temperature when the effect of temperature on the tensile properties are known.

Based on the results in the previous sections the following relation between CTOD and gross stress level is proposed:

$$\frac{\delta}{\delta_0} = b \left[\exp \left(d \frac{\sigma_G}{\sigma_y} \right) - 1 \right] \quad (4)$$

where δ_0 is a reference CTOD equal to 0.25 mm, which is a minimum required CTOD when applicable according to [37]. b and d are functions of yield stress and Lüders strain. Values for b and d in Eq. 4 were found by fitting the proposed relation to the numerical results shown in Figs. 6 and 7, and based on these results the following relation for b is proposed:

$$b = \begin{cases} \left(23.4 \frac{\sigma_y}{\sigma_0} + 2.7 \right) \times 10^{-3} & \text{if } \varepsilon_L = 0 \\ \left(23.2 \frac{\sigma_y}{\sigma_0} - 1.1 \right) \times 10^{-3} & \text{if } 0 < \varepsilon_L \leq 1\% \\ \left(21.6 \frac{\sigma_y}{\sigma_0} - 0.6 \right) \times 10^{-3} & \text{if } 1\% < \varepsilon_L \leq 5\% \end{cases} \quad (5)$$

where b is a function of the yield stress normalized by a reference stress (σ_0) equal to 420 MPa, which is the specified minimum yield strength (SMYS) for many construction steels. As Fig. 7 suggests, the effect of Lüders strain is evident, and it is thus accounted for in Eq. 5 by dividing the equation into three separate parts, where the first part is valid for materials showing no Lüders behavior, the second part is valid for Lüders strains below 1%, and the third part is valid for larger Lüders strains up to 5%. This partitioning of Eq. 5 helps estimating the CTOD more precisely for various levels of Lüders strain. The proposed relation

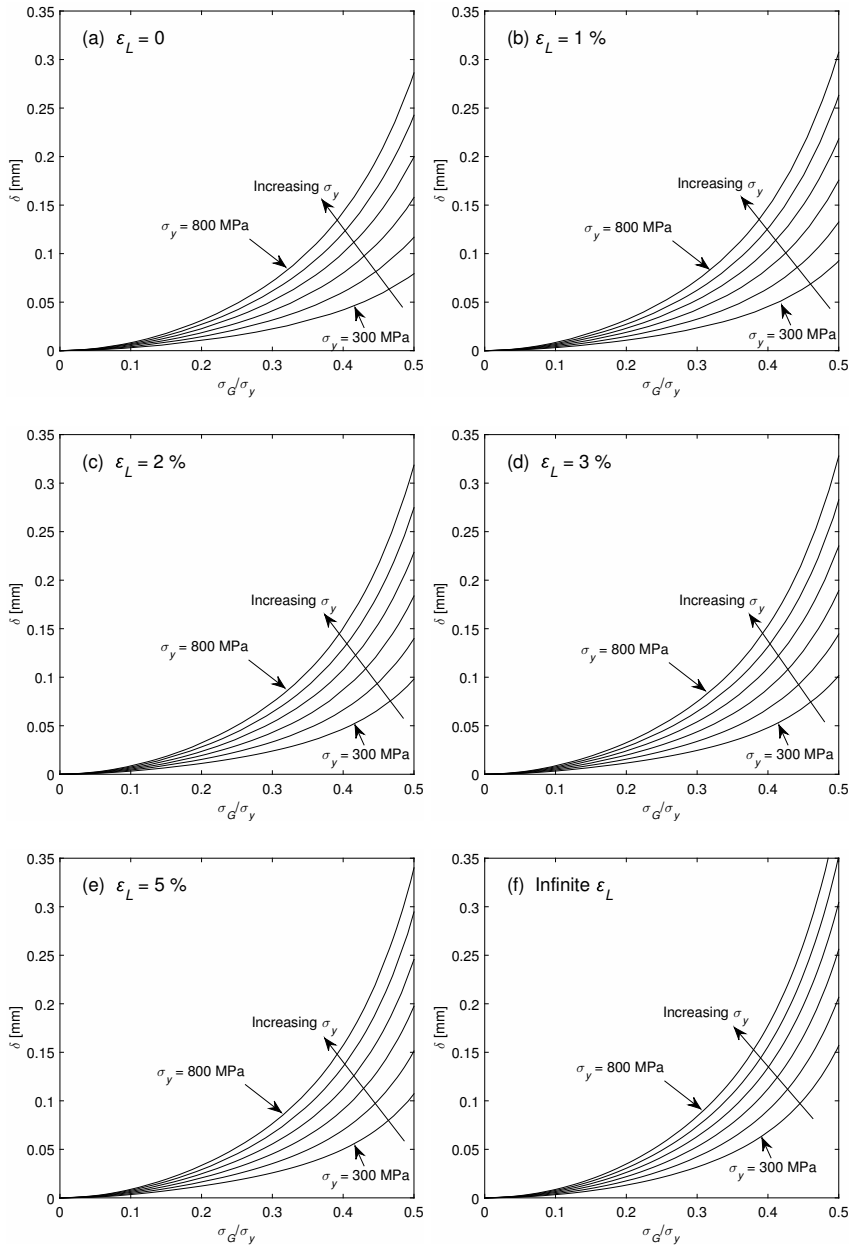


Fig. 6. CTOD versus gross stress level with 300 MPa to 800 MPa yield strengths and Lüders strains ranging from 0 to infinite in (a) to (f) respectively.

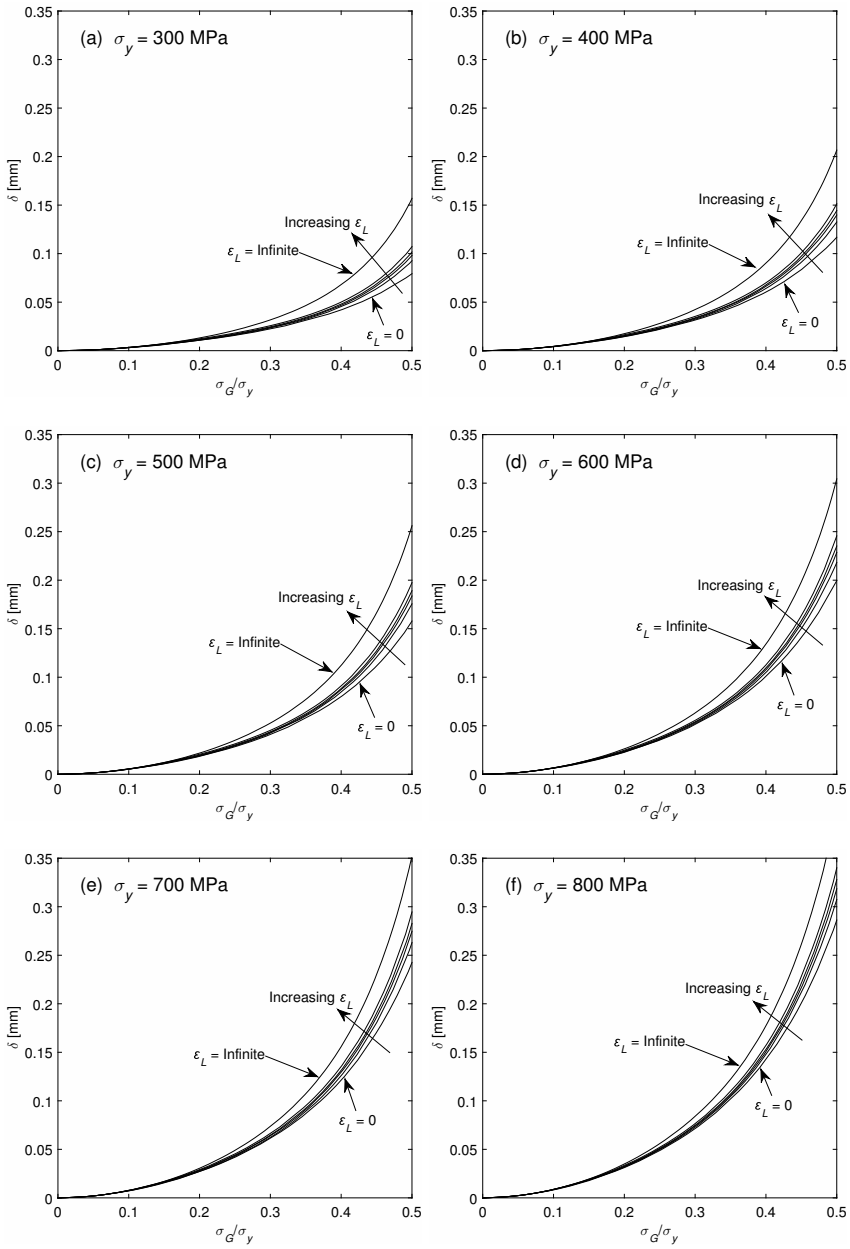


Fig. 7. CTOD versus gross stress level with 0, 1%, 2%, 3%, 5% and infinite Luders strains and yield strengths ranging from 300 MPa to 800 MPa in (a) to (f) respectively.

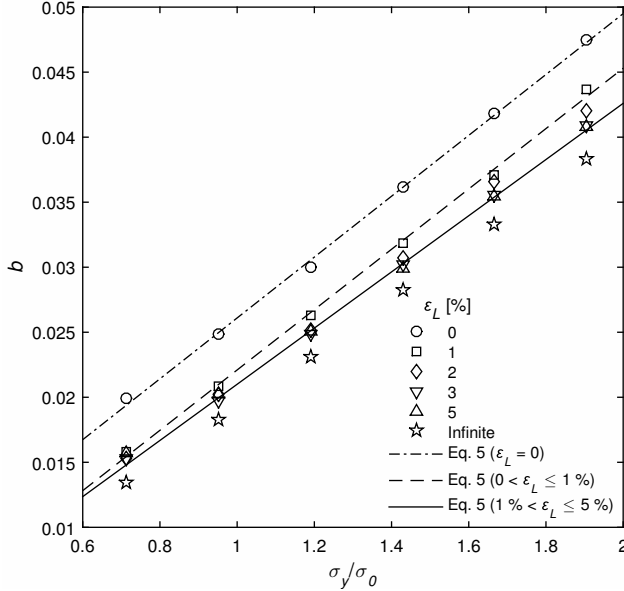


Fig. 8. Proposed relations according to Eq. 5 as a function of yield strength normalized by a reference stress of 420 MPa together with the values for the b -parameter obtained by fitting the proposed relation in Eq. 4 to the numerical results shown in Figs. 6 and 7.

for b as a function of σ_y/σ_0 is shown in Fig. 8 together with the values for b according to the fitting of Eq. 4 to the numerical results.

Based on the values for d found by fitting Eq. 4 to the numerical results, the following relation is proposed:

$$d = \begin{cases} -0.51 \left(\frac{\sigma_y}{\sigma_0} \right)^2 + 1.97 \frac{\sigma_y}{\sigma_0} + 4.52 & \text{if } 0 \leq \varepsilon_L < 1\% \\ -0.33 \left(\frac{\sigma_y}{\sigma_0} \right)^2 + 1.17 \frac{\sigma_y}{\sigma_0} + A & \text{if } 1\% \leq \varepsilon_L \leq 5\% \end{cases} \quad (6)$$

where d is a function of yield strength normalized by the reference stress of 420 MPa. d is dependent on the amount of Lüders strain, and A is a function of Lüders strain. Similar to Eq. 5, the partitioning of Eq. 6 into two Lüders strain ranges helps estimating the CTOD more precisely for various levels of Lüders strain. Based on the fitting of Eq. 6 to the values for d found by fitting Eq. 4 to the numerical results, the following relation between A and ε_L is proposed:

$$A = \frac{6.025}{1 + 0.106 \exp(-58\varepsilon_L)} \quad (7)$$

The proposed relation between A and ε_L is shown in Fig. 9 together with the values for A , which were found by fitting the relation from Eq. 7 to the numerical results. The proposed relation for d in Eq. 6 using the calculated values for A according to Eq. 7 is shown in Fig. 10 as a function of yield stress normalized by the reference stress together with the values for d according to the fitting of Eq. 4 to the numerical results.

The model described by the proposed relations in Eqs. 4, 5, 6 and 7 are compared to numerical results by coupling the model to the effect of temperature on the tensile properties. This is done by varying the yield strength and Lüders strain in the model material according to Eqs. 1 and 2 respectively at

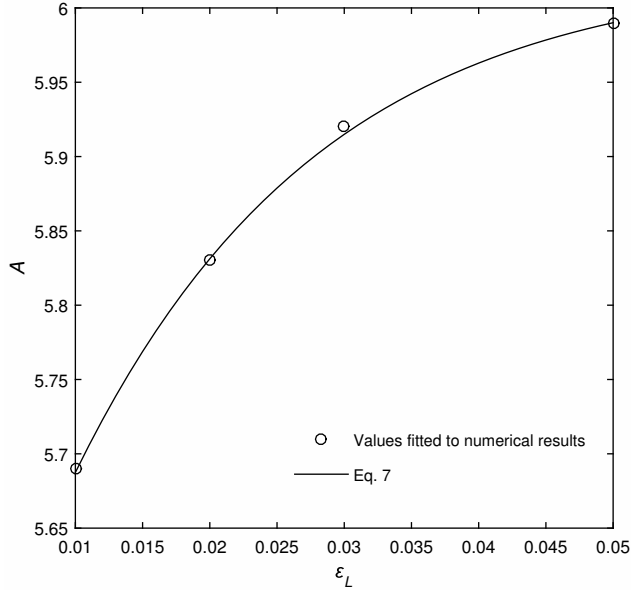


Fig. 9. Comparison between Eq. 7 and the values for A from the fitting of Eq. 6 to the numerical results.

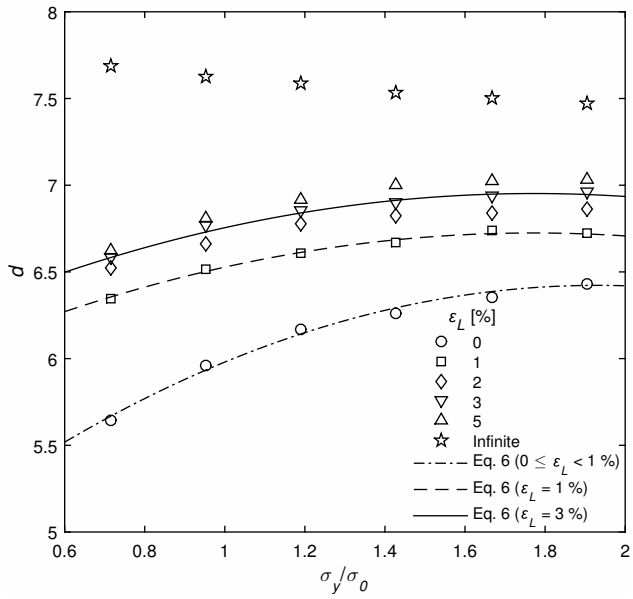


Fig. 10. Proposed relations according to Eqs. 6 and 7 as a function of yield strength normalized by a reference stress of 420 MPa together with the values for the d -parameter obtained by fitting the proposed relation in Eq. 4 to the numerical results shown in Figs. 6 and 7.

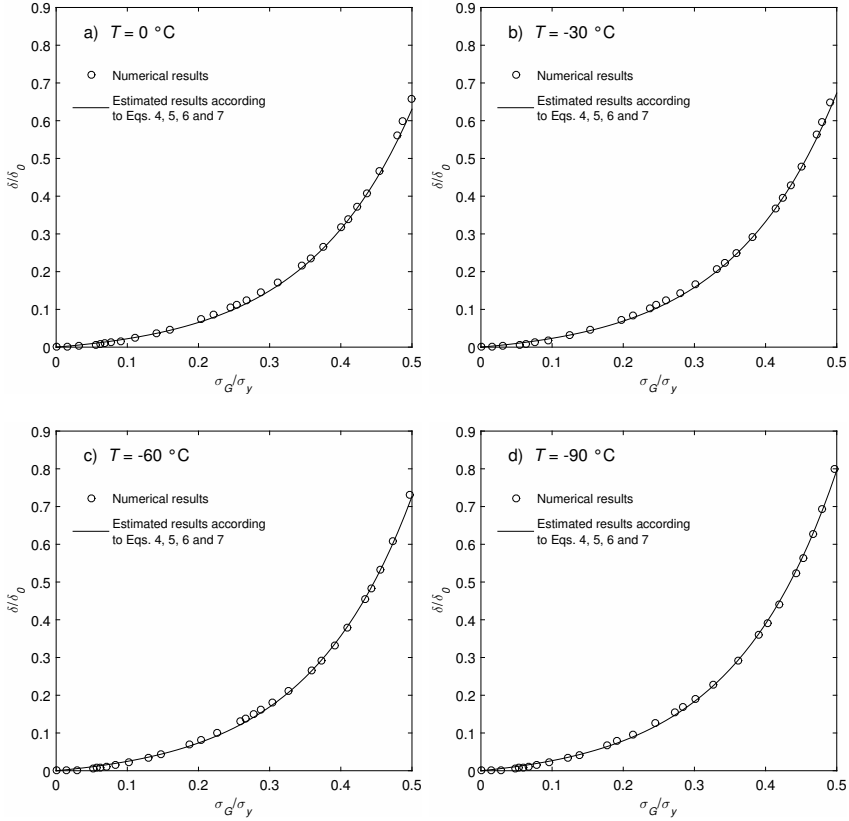


Fig. 11. Proposed temperature dependent relation according to Eqs. 4, 5, 6 and 7 between CTOD and applied gross stress level in the SENT specimen compared to numerical results at (a) 0 °C, (b) -30 °C, (c) -60 °C and (d) -90 °C.

four different temperatures. The temperatures used are the same as during the experimental tensile tests in [9]. The comparison between the estimated and the numerical results is shown in Fig. 11, where the normalized CTOD is plotted versus the applied gross stress level. The estimated results for the four different temperatures are compared in Fig. 12. The gross stress levels are calculated as the gross stress divided by the estimated yield stresses according to Eq. 1 at the respective temperatures.

Figs. 11 and 12 indicate that the proposed relations can be used to estimate the CTOD at different temperatures quite accurately for the material model used in this study. The proposed CTOD model utilizes known temperature dependent behavior of the yield strength and Lüders strain to estimate the CTOD in a SENT specimen at different temperatures and gross stress levels. The model may also be modified to estimate the CTOD for other geometries, such as for cracks in pipelines in Arctic conditions. The model should also be sufficient to use for other similar materials if their tensile behavior is comparable and the effect of temperature on the tensile behavior is known.

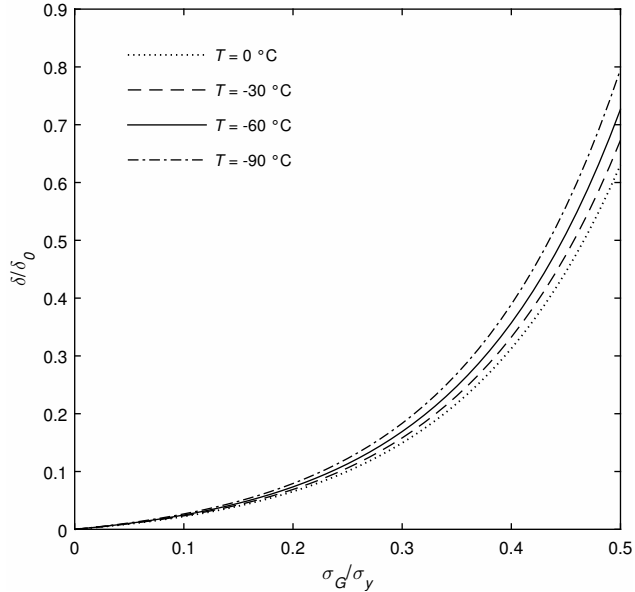


Fig. 12. Comparison between CTOD curves estimated using the proposed CTOD model at four different temperatures.

5. Conclusion

The effects of temperature dependent tensile properties on the crack driving force in a SENT specimen have been studied numerically, and an approximate model that predicts the CTOD based on tensile properties, temperature and loading is proposed. The SENT specimen studied has crack depth $a/W = 0.5$, and the material model is based on experimental results. The gross stress levels applied in this work are $\sigma_G/\sigma_y \leq 0.5$.

The yield strength and Lüders strain are both usually increasing with decreasing temperature. In this work it is shown that increasing yield strength results in increased crack driving force in terms of CTOD for given gross stress levels. It is also shown that increasing Lüders strain results in increased CTOD. The crack driving force is thus increasing with decreasing temperature at given gross stress levels.

The proposed approximate CTOD model is based on the numerical results, and it is found to give quite accurate results when compared to numerical results using the same geometry, loading and material model as used in this work. The model may also be modified to predict the CTOD for other similar geometries and materials at different temperatures. This can for instance make it useful in estimating the CTOD based on temperature and loading for a crack in a pipeline in Arctic conditions.

The topics of this work can be further studied, where by other things the effect of geometry and crack tip constraint on the proposed model can be investigated, as only one geometry was studied in this work. This may result in a universal model that can be used to predict the crack driving force for many different geometries and applications. Also the effect of plastic hardening behavior can be studied in more detail, as this work only considers a single hardening curve for all material models.

Acknowledgements

The authors wish to thank the Research Council of Norway for funding through the Petromaks 2 Programme, Contract No.228513/E30. The financial support from ENI, Statoil, Lundin, Total, JFE Steel

Corporation, Posco, Kobe Steel, SSAB, Bredero Shaw, Borealis, Trelleborg, Nexans, Aker Solutions, FMC Kongsberg Subsea, Kværner Verdal, Marine Aluminium, Hydro and Sapa are also acknowledged.

References

- [1] D. L. Gautier, K. J. Bird, R. R. Charpentier, A. Grantz, D. W. Houseknecht, T. R. Klett, T. E. Moore, J. K. Pitman, C. J. Schenk, J. H. Schuenemeyer, Assessment of undiscovered oil and gas in the Arctic, *Science* 324 (5931) (2009) 1175–1179.
- [2] O. M. Akselsen, E. Østby, B. Nyhus, Low temperature fracture toughness of X80 girth welds, in: *The Twenty-second International Offshore and Polar Engineering Conference, International Society of Offshore and Polar Engineers*, 2012, pp. 283–289.
- [3] O. M. Akselsen, E. Østby, C. Thaulow, Low temperature toughness in SA welding of 420 MPa steel, in: *The Twenty-first International Offshore and Polar Engineering Conference, International Society of Offshore and Polar Engineers*, 2011, pp. 414–420.
- [4] J.-H. Baek, Y.-P. Kim, W.-S. Kim, Y.-T. Kho, Effect of temperature on the charpy impact and CTOD values of type 304 stainless steel pipeline for LNG transmission, *KSME International Journal* 16 (8) (2002) 1064–1071.
- [5] L. S. Costin, J. Duffy, The effect of loading rate and temperature on the initiation of fracture in a mild, rate-sensitive steel, *Journal of Engineering Materials and Technology* 101 (3) (1979) 258–264.
- [6] A. S. Eldin, S. C. Collins, Fracture and yield stress of 1020 steel at low temperatures, *Journal of Applied Physics* 22 (10) (1951) 1296.
- [7] E. Heier, E. Østby, O. M. Akselsen, Reeling installation of rigid steel pipelines at low temperature, in: *The Twenty-third International Offshore and Polar Engineering Conference, International Society of Offshore and Polar Engineers*, 2013, pp. 265–269.
- [8] A. Marais, M. Mazière, S. Forest, A. Parrot, P. Le Delliou, Identification of a strain-aging model accounting for Lüders behavior in a C-Mn steel, *Philosophical Magazine* 92 (28-30) (2012) 3589–3617.
- [9] X. Ren, H. O. Nordhagen, Z. Zhang, O. M. Akselsen, Tensile properties of 420 MPa steel at low temperature, in: *The Twenty-fifth International Offshore and Polar Engineering Conference, International Society of Offshore and Polar Engineers*, 2015, pp. 346–352.
- [10] R. O. Ritchie, J. F. Knott, J. R. Rice, On the relationship between critical tensile stress and fracture toughness in mild steel, *Journal of the Mechanics and Physics of Solids* 21 (6) (1973) 395–410.
- [11] C. F. Robertson, K. Obrtlík, B. Marini, Dislocation structures in 16MND5 pressure vessel steel strained in uniaxial tension at different temperatures from -196°C up to 25°C , *Journal of Nuclear Materials* 366 (1-2) (2007) 58–69.
- [12] H. Sieurin, R. Sandström, Fracture toughness of a welded duplex stainless steel, *Engineering Fracture Mechanics* 73 (4) (2006) 377–390.
- [13] W. A. Sorem, R. H. Dodds Jr, S. T. Rolfe, Effects of crack depth on elastic-plastic fracture toughness, *International Journal of Fracture* 47 (2) (1991) 105–126.
- [14] M. L. Wilson, R. H. Hawley, J. Duffy, The effect of loading rate and temperature on fracture initiation in 1020 hot-rolled steel, *Engineering Fracture Mechanics* 13 (2) (1980) 371–385.
- [15] A. H. Cottrell, B. A. Bilby, Dislocation theory of yielding and strain ageing of iron, *Proceedings of the Physical Society of London Section A* 62 (349) (1949) 49–62.
- [16] G. T. Hahn, A model for yielding with special reference to the yield-point phenomena of iron and related bcc metals, *Acta Metallurgica* 10 (8) (1962) 727–738.
- [17] J. F. Hallai, S. Kyriakides, Underlying material response for Lüders-like instabilities, *International Journal of Plasticity* 47 (2013) 1–12.
- [18] D. H. Johnson, Lüders bands in RPV steel, PhD thesis, Cranfield University (2013).
- [19] Y. Liu, S. Kyriakides, J. F. Hallai, Reeling of pipe with Lüders bands, *International Journal of Solids and Structures* 72 (2015) 11–25.
- [20] M. Mazière, S. Forest, Strain gradient plasticity modeling and finite element simulation of Lüders band formation and propagation, *Continuum Mechanics and Thermodynamics* 27 (1-2) (2013) 83–104.
- [21] N. Tsuchida, Y. Tomota, K. Nagai, K. Fukaura, A simple relationship between Lüders elongation and work-hardening rate at lower yield stress, *Scripta Materialia* 54 (1) (2006) 57–60.
- [22] U. Zerbst, R. A. Ainsworth, H. T. Beier, H. Pisarski, Z. L. Zhang, K. Nikbin, T. Nitschke-Pagel, S. Munstermann, P. Kucharczyk, D. Klingbeil, Review on fracture and crack propagation in weldments - a fracture mechanics perspective, *Engineering Fracture Mechanics* 132 (2014) 200–276.
- [23] E. Østby, O. M. Akselsen, M. Hauge, A. M. Horn, Fracture mechanics design criteria for low temperature applications of steel weldments, in: *The Twenty-third International Offshore and Polar Engineering Conference, International Society of Offshore and Polar Engineers*, 2013, pp. 315–321.
- [24] B. Nyhus, M. L. Polanco, O. Ørjasæter, SENT specimens an alternative to SENB specimens for fracture mechanics testing of pipelines, in: *ASME 2003 22nd International Conference on Offshore Mechanics and Arctic Engineering, American Society of Mechanical Engineers*, 2003, pp. 259–266.
- [25] Det Norske Veritas, Recommended practice DNV-RP-F108: Fracture control for pipeline installation methods introducing cyclic plastic strain (January 2006).
- [26] British Standards Institution, BS 7910: Guide to methods for assessing the acceptability of flaws in metallic structures (2013).
- [27] Dassault Systèmes Simulia Corp., Abaqus 6.14 (2014).

-
- [28] T. Shioya, J. Shioiri, Elastic-plastic analysis of the yield process in mild steel, *Journal of the Mechanics and Physics of Solids* 24 (4) (1976) 187–204.
- [29] H. Tsukahara, T. Iung, Finite element simulation of the Piobert–Lüders behavior in an uniaxial tensile test, *Materials Science and Engineering: A* 248 (1–2) (1998) 304–308.
- [30] M. R. Wenman, P. R. Chard-Tuckey, Modelling and experimental characterisation of the Lüders strain in complex loaded ferritic steel compact tension specimens, *International Journal of Plasticity* 26 (7) (2010) 1013–1028.
- [31] Y. T. Zhang, J. L. Qiao, T. Ao, Strain softening of materials and Lüders-type deformations, *Modelling and Simulation in Materials Science and Engineering* 15 (2) (2007) 147–156.
- [32] P. A. Eikrem, Z. L. Zhang, B. Nyhus, Effect of plastic prestrain on the crack tip constraint of pipeline steels, *International Journal of Pressure Vessels and Piping* 84 (12) (2007) 708–715.
- [33] J. Liu, Z. L. Zhang, B. Nyhus, Residual stress induced crack tip constraint, *Engineering Fracture Mechanics* 75 (14) (2008) 4151–4166.
- [34] C. Thaulow, E. Østby, B. Nyhus, Z. L. Zhang, B. Skallerud, Constraint correction of high strength steel: Selection of test specimens and application of direct calculations, *Engineering Fracture Mechanics* 71 (16–17) (2004) 2417–2433.
- [35] J. Xu, Z. L. Zhang, E. Østby, B. Nyhus, D. B. Sun, Effects of crack depth and specimen size on ductile crack growth of SENT and SENB specimens for fracture mechanics evaluation of pipeline steels, *International Journal of Pressure Vessels and Piping* 86 (12) (2009) 787–797.
- [36] J. Xu, Z. L. Zhang, E. Østby, B. Nyhus, D. B. Sun, Constraint effect on the ductile crack growth resistance of circumferentially cracked pipes, *Engineering Fracture Mechanics* 77 (4) (2010) 671–684.
- [37] Standard Norge, NORSOK M-120: Material data sheets for structural steels (2008).